Evaluation of bacterial glycerol dialkyl glycerol tetraether and ^{2}H-^{18}O biomarker proxies along a Central European topsoil transect

Johannes Hepp[1,2,*], Imke Kathrin Schäfer[3], Verena Lanny[4], Jörg Franke[3],

Marcel Bliedtner[3,a], Kazimierz Rozanski[5], Bruno Glaser[2], Michael Zech[2,6],

Timothy Ian Eglinton[4], Roland Zech[3,a]

[1]Chair of Geomorphology and BayCEER, University of Bayreuth, 95440 Bayreuth, Germany and

[2]Institute of Agronomy and Nutritional Sciences, Soil Biogeochemistry, Martin-Luther-University Halle-Wittenberg, 06120 Halle, Germany

[3]Institute of Geography and Oeschger Centre for Climate Change Research, University of Bern, 3012 Bern, Switzerland

[4]Department of Earth Science, ETH Zurich, 8092 Zurich, Switzerland

[5]Faculty of Physics and Applied Computer Science, AGH University of Science and Technology, 30-059 Kraków, Poland

[6]Institute of Geography, Faculty of Environmental Sciences, Technical University of Dresden, 01062 Dresden, Germany

[a]now at Institute of Geography, Chair of Physical Geography, Friedrich-Schiller University of Jena, 07743 Jena, Germany

*corresponding author (johannes-hepp@gmx.de)

Keywords

Leaf wax n-alkanes, hemicellulose sugars, pH, temperature, CBT, MBT', δ^2H and $\delta^{18}O$, relative humidity

Abstract

Molecular fossils, like bacterial branched glycerol dialkyl glycerol tetraethers (brGDGTs), and the stable isotopic composition of biomarkers, such as δ^2H of leaf wax-derived n-alkanes ($\delta^2H_{n\text{-alkane}}$) or $\delta^{18}O$ of hemicellulose-derived sugars ($\delta^{18}O_{sugar}$) are increasingly used for the reconstruction of past climate and environmental conditions. Plant-derived $\delta^2H_{n\text{-alkane}}$ and $\delta^{18}O_{sugar}$ values record the isotopic composition of plant source water ($\delta^2H_{source\text{-water}}$ and $\delta^{18}O_{source\text{-water}}$), which usually reflects mean annual precipitation ($\delta^2H_{precipiation}$ and $\delta^{18}O_{precipiation}$), modulated by evapotranspirative leaf water enrichment and biosynthetic fractionation (ε_{bio}). Accuracy and precision of respective proxies should be ideally evaluated at a regional scale. For this study, we analysed topsoils below coniferous and deciduous forests, as well as grassland soils along a Central European transect in order to investigate the variability and robustness of various proxies, and to identify effects related to vegetation. Soil pH-values derived from brGDGTs correlate reasonably well with measured soil pH-values, but systematically overestimate them ($\Delta pH = 0.6 \pm 0.6$). The branched vs. isoprenoid tetraether index (BIT) can give some indication whether the pH reconstruction is reliable. Temperatures derived from brGDGTs overestimate mean annual air temperatures slightly ($\Delta T_{MA} = 0.5°C \pm 2.4$). Apparent isotopic fractionation ($\varepsilon_{n\text{-alkane/precipitation}}$ and $\varepsilon_{sugar/precipitation}$) is lower for grassland sites than for forest sites due to "signal damping", i.e. grass biomarkers do not record the full evapotranspirative leaf water enrichment. Coupling $\delta^2H_{n\text{-alkane}}$ with $\delta^{18}O_{sugar}$ allows to reconstruct the stable isotopic composition of the source water more accurately than without the coupled approach ($\Delta\delta^2H = \sim-21‰ \pm 22$ and $\Delta\delta^{18}O = \sim-2.9‰ \pm 2.8$). Similarly, relative humidity during daytime and vegetation period (RH_{MDV}) can be reconstructed using the coupled isotope approach ($\Delta RH_{MDV} = \sim-17 \pm 12$). Especially for coniferous sites, reconstructed RH_{MDV} values as well as source water isotope composition underestimate the measured values. This can be likely explained by understory grass vegetation at the coniferous sites contributing significantly to the n-alkane pool but only marginally to the sugar pool in the topsoils. Vegetation-dependent variable "signal damping" and ε_{bio} (regarding ^2H between n-alkanes and leaf water) along our European transect are difficult to quantify but likely contribute to the observed underestimation in the source water isotope composition and RH reconstructions. Microclimate variability could cause the rather large uncertainties. Vegetation-related effects do, by contrast, not affect the brGDGT-derived reconstructions. Overall, GDGTs and the coupled $\delta^2H_{n\text{-alkane}}$-$\delta^{18}O_{sugar}$ approach have great potential for more quantitative paleoclimate reconstructions.

1 Introduction

Information about the variability and consequences of past climate changes is a prerequisite for precise predictions regarding the present climate change. Molecular fossils, so called biomarkers, have great potential to enhance our understanding about variations of past climate and environmental changes. Lipid biomarkers in particular are increasingly used for paleoclimate and environmental reconstructions (e.g. Brincat et al., 2000; Eglinton and Eglinton, 2008; Rach et al., 2014; Romero-Viana et al., 2012; Schreuder et al., 2016). However strengths and limitations of respective proxies need to be known (Dang et al., 2016). For this, calibrations using modern reference samples are essential.

One famous and widely applied lipid biomarker group are terrestrial branched glycerol dialkyl glycerol tetraethers (brGDGTs). They are synthesized in the cell membranes of anaerobe heterotrophic soil bacteria (Oppermann et al., 2010; Weijers et al., 2010) have great potential for the reconstruction of past environmental conditions (e.g. Coffinet et al., 2017; Schreuder et al., 2016; Zech et al., 2012), although some uncertainties exist. Calibration studies suggest that the relative abundance of the individual brGDGTs varies with mean annual air temperature (T_{MA}) and soil pH (Peterse et al., 2012; Weijers et al., 2007), at least across large, global climate gradients or along pronounced altitudinal gradients (Wang et al., 2017). However, in arid regions the production of brGDGT is limited, while isoprenoidal GDGTs (iGDGTs) produced by archaea provide the dominant part of the overall soil GDGT pool (Anderson et al., 2014; Dang et al., 2016; Dirghangi et al., 2013; Wang et al., 2013; Xie et al., 2012). The ratio of brGDGTs vs. isoprenoid GDGTs (BIT) can be used as indication whether a reconstruction of T_{MA} and pH will be reliable. Moreover, Mueller-Niggemann et al. (2016) revealed an influence of the vegetation cover on the brGDGT producing soil microbes. From field experiments, it is known that vegetation type and mulching practice strongly effect soil temperature and moisture (Awe et al., 2015; Liu et al., 2014). Thus, multiple factors can be expected to influence soil microbial communities and GDGT production. So far, little is known about the variability of GDGT proxies on a regional scale, and a calibration study with small climate gradient but with different vegetation types might be useful.

Concerning paleohydrology proxies, compound-specific stable hydrogen isotopes of leaf wax biomarkers, such as long chain n-alkanes ($\delta^2H_{n\text{-alkanes}}$) record the isotopic signal of precipitation and therefore past climate and environmental conditions (Sachse et al., 2004, 2006). However, various influencing factors are known e.g. the moisture source to leaf waxes (Pedentchouk and Zhou, 2018 and Sachse et al., 2012 for review). Next is the evapotranspiration of leaf water (Feakins and Sessions, 2010; Kahmen et al., 2013; Zech et al., 2015), which is strongly driven by relative air humidity (RH; e.g. Cernusak et al., 2016 for review). In addition, a strong precipitation signal is known to be incorporated into long chain leaf waxes (Hou et al., 2008; Rao et al., 2009; Sachse et al., 2004). In paleoclimate studies, it is often not feasible to disentangle between the evapotranspirative enrichment from the precipitation signal. Zech et al. (2013) proposed to couple $\delta^2H_{n\text{-alkane}}$ results with oxygen stable isotopes of hemicellulose-derived sugars ($\delta^{18}O_{sugar}$). Assuming constant biosynthetic fractionation (ε_{bio}) for the different compound classes (n-alkanes and hemicellulose sugars), this coupling enables the reconstruction of the isotopic composition of leaf water, RH, δ^2H and $\delta^{18}O$ of plant source water ($\approx \delta^2H$ and $\delta^{18}O$ of precipitation; Tuthorn et al., 2015). So far, a detailed evaluation of this

99   approach on the European scale, as well as related effects concerning vegetation changes is
100   missing.

101   We analysed topsoil samples under coniferous, deciduous and grassland vegetation along a
102   Central European transect in order to estimate the variability of the biomarker proxies. More
103   specifically, we aim to test whether:

104   (i) the vegetation type has an influence on the brGDGT proxies, the $\delta^2H_{n\text{-alkane}}$ and the $\delta^{18}O_{sugar}$
105   stable isotopic composition, as well as on reconstructed $\delta^2H_{source\text{-water}}$, $\delta^{18}O_{source\text{-water}}$ and RH.

106   (ii) the published brGDGT proxies used for reconstructing mean annual temperature and soil
107   pH are sensitive enough to reflect the medium changes in temperature and soil pH along our
108   transect.

109   (iii) the coupled $\delta^2H_{n\text{-alkane}}$-$\delta^{18}O_{sugar}$ approach enables a δ^2H and $\delta^{18}O$ of precipitation and RH
110   reconstruction along the transect.

111

2 Material and methods

2.1 Geographical setting and sampling

114   In November 2012, we collected 29 topsoil samples (0-5 cm depth) from 16 locations along a
115   transect from Southern Germany to Southern Sweden (Fig. 1A). We distinguished between sites
116   with coniferous forest (con, n = 9), deciduous forest (dec, n = 14) and grassland (grass, n = 6)
117   vegetation cover (for more details see Schäfer et al. (2016) and Tab. S1).

118

2.2 Database of instrumental climate variables and isotope composition of precipitation

120   Climate data was derived from close-by weather observation stations operating by the regional
121   institutions (Deutscher Wetterdienst (DWD) for Germany, Danmarks Meteorologiske Institut
122   (DMI) for Denmark and the Sveriges Meteorologiska och Hydrologiska Institute (SMHI) for
123   Sweden). The DWD provides hourly data for each station (DWD Climate Data Center, 2018b),
124   enabling not only the calculation of T_{MA}, but also of the mean annual relative air humidity
125   (RH_{MA}), mean temperature and relative air humidity during the vegetation period (T and
126   RH_{MV}), and of daytime temperature and relative humidity averages over the vegetation period
127   (T and RH_{MDV}). In addition, annual precipitation observations were used to derive the mean
128   annual precipitation amount (P_{MA}; DWD Climate Data Center, 2018b). From the DMI, the
129   respective climate variables were derived from published technical reports (Cappelen, 2002;
130   Frich et al., 1997; Laursen et al., 1999). The SMHI provides open data from which we derived
131   the climate variables for the Swedish sites (Swedish Meteorological and Hydrological Institute,
132   2018). For more details about the climate database used for calculations and comparisons, the
133   reader is referred to Tab. S2.

134   For comprising German precipitation (δ^2H and $\delta^{18}O$) along the transect, we realized a
135   regionalisation (called δ^2H_{GIPR} and $\delta^{18}O_{GIPR}$) using online available data from 34 German GNIP
136   stations, 4 Austrian ANIP stations and the Groningen GNIP station (van Geldern et al., 2014;
137   IAEA/WMO, 2018; Stumpp et al., 2014; Umweltbundesamt GmbH, 2018), following the
138   approach of Schlotter (2007). However, instead of the multivariate regression procedure applied

139   by Schlotter (2007), we used a random forest approach (Hothorn et al., 2006; Strobl et al., 2007,
140   2008) to describe the relationship of squared latitude, latitude, longitude and altitude vs. long
141   term weighted means of precipitation δ^2H and $\delta^{18}O$, and realized the prediction for each site
142   (see supplementary method description for more information). For the Danish and Swedish
143   sites, such a procedure was not possible. Hence, the annual precipitation δ^2H and $\delta^{18}O$ values
144   were derived from the Online Isotopes in Precipitation Calculator (OIPC, version 3.1), therefore
145   called δ^2H_{OIPC} and $\delta^{18}O_{OIPC}$ (Bowen, 2018; Bowen and Revenaugh, 2003; IAEA/WMO, 2015).
146   The finally used $\delta^2H_{GIPR,OIPC}$ and $\delta^{18}O_{GIPR,OIPC}$ data are given in Tab. S1.

147   The T_{MA} along the transect ranges from 5.3 to 10.6°C, and P_{MA} ranges from 554 to 1769 mm
148   (Fig. 1B). Precipitation δ^2H and $\delta^{18}O$ shows moderate changes along the transect, $\delta^2H_{GIPR,OIPC}$
149   varies between -52 and -79‰, and $\delta^{18}O_{GIPR,OIPC}$ ranges from -7.4 to -10.9‰ (Fig. 1C).

150   Correlations between $\delta^{18}O_{GIPR,OIPC}$ and P_{MA}, altitude of the locations, T_{MA} are given in the
151   supplementary material (Fig. S1 to S3), along with a $\delta^2H_{GIPR,OIPC}$ vs. $\delta^{18}O_{GIPR,OIPC}$ scatter plot
152   (Fig. S4).
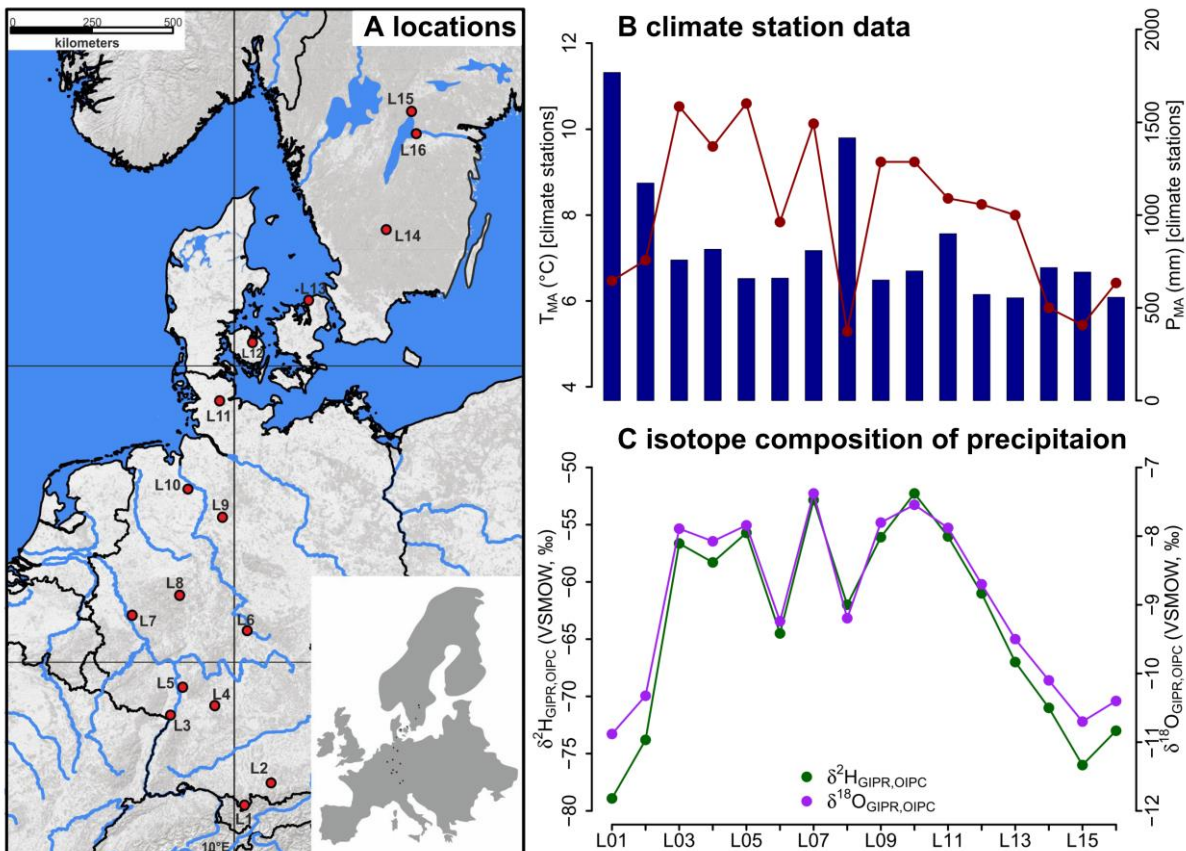
153
154   **Fig. 1.** (A) Sample locations (red dots, map source: US National Park Service), (B) variations
155   of mean annual air temperature (T_{MA}, red dots and line) and mean annual precipitation (P_{MA},
156   blue bars) derived from close-by climate station data, and (C) hydrogen and oxygen stable
157   isotope composition of precipitation ($\delta^2H_{GIPR,OIPC}$ and $\delta^{18}O_{GIPR,OIPC}$, respectively) as derived for
158   the sampled transect locations (see section 2.2 GIPR δ^2H and $\delta^{18}O$ generation procedure). The
159   reader is referred to section 2.2 (and Tab. S1 and S2) for database and reference information of
160   data plotted in (B) and (C).

161

2.3 Soil extractions and analysis

2.3.1 GDGTs and pH

A detailed description of sample preparation for lipid analysis can be found in Schäfer et al. (2016). Briefly, 1–6 g freeze-dried and grounded soil sample was microwave extracted with 15 ml dichloromethane (DCM)/methanol (MeOH) 9:1 *(v:v)* at 100°C for 1 h. Extracts were separated over aminopropyl silica gel (Supelco, 45 μm) pipette columns. The nonpolar fraction (including *n*-alkanes) was eluted with hexane and further purified over $AgNO_3$ coated silica pipette columns (Supelco, 60-200 mesh) and zeolite (Geokleen Ltd.). The GDGT-containing fraction was eluted with DCM:MeOH 1:1 *(v:v)*, re-dissolved in hexane/isopropanol (IPA) 99:1 *(v:v)* and transferred over 0.45 μm PTFE filters into 300 μl inserts. For quantification, a known amount of a C_{46} diol standard was added after transfer. The samples were analysed at ETH Zurich using an Agilent 1260 Infinity series HPLC–atmospheric chemical pressure ionization mass spectrometer (HPLC-APCI-MS) equipped with a Grace Prevail Cyano column (150 mm × 2.1 mm; 3 μm). The GDGTs were eluted isocratically with 90% A and 10% B for 5 min and then with a linear gradient to 18% B for 34 min at 0.2 ml min^{-1}, where A=hexane and B=hexane/isopropanol (9:1, *v:v*). Injection volume was 10 μl and single ion monitoring of $[M+H]^+$ was used to detect GDGTs.

The pH of the samples was measured in the laboratory of the Soil Biogeochemistry group, Institute of Agronomy and Nutritional Sciences, Martin-Luther-University Halle-Wittenberg, using a pH meter in a 1:3 soil:water *(w/v)* mixture.

2.3.2 $\delta^2H_{n\text{-alkane}}$

The hydrogen isotopic composition of the highest concentrated *n*-alkanes (*n*-C_{25}, *n*-C_{27}, *n*-C_{29}, *n*-C_{31}, and *n*-C_{33}) was determined using a TRACE GC Ultra Gas Chromatography connected to a Delta V Plus Isotope Ratio Mass Spectrometer via a ^2H pyrolysis reactor kept at 1420 °C (GC-^{2}H-Py-IRMS; Thermo Scientific, Bremen, Germany) at ETH Zurich (Christoph et al., 2019). For more details about *n*-alkane quantification the reader is refereed to Schäfer et al. (2016). The compound-specific $^2H/^1H$ ratios were calibrated against an external standard with $C_{15} - C_{35}$ homologues. External standard mixtures (A4 mix from A. Schimmelmann, University of Indiana) were run between the samples for multipoint linear normalization. The H^+_3 factor was determined on each measurement day and was constant throughout the periods of the sample batches. Samples were analysed in duplicates, and results typically agreed within 4% (average difference = 1.4%). All δ^2H values are expressed relative to the Vienna Standard Mean Ocean Water (V-SMOW).

2.3.3 $\delta^{18}O_{sugar}$

Hemicellulose sugars were extracted and purified using a slightly modified standard procedure (Amelung et al., 1996; Guggenberger et al., 1994; Zech and Glaser, 2009). Briefly, myoinositol was added to the samples prior to extraction as first internal standard. The sugars were released hydrolytically using 4M trifluoroacetic acid for 4 h at 105°C, cleaned over glass fibre filters and further purified using XAD and Dowex columns. Before derivatization with methylboronic acid (Knapp, 1979), the samples were frozen, freeze-dried, and 3-O-methylglucose in dry pyridine

was added as second internal standard. Compound-specific hemicellulose sugar ^{18}O measurements were performed in the laboratory of the Soil Biogeochemistry group, Institute of Agronomy and Nutritional Sciences, Martin-Luther-University Halle-Wittenberg, using GC-^{18}O-Py-IRMS (all devices from Thermo Fisher Scientific, Bremen, Germany). Standard deviations of the triplicate measurements were 1.4‰ (over 29 investigated samples) for arabinose and xylose, respectively. We focus on these two hemicellulose-derived neutral sugars arabinose and xylose as they strongly predominate over fucose in terrestrial plants, soils and sediments (Hepp et al., 2016 and references therein). Rhamnose concentrations were too low to obtain reliable $\delta^{18}O$ results. All $\delta^{18}O$ values are expressed relative to the Vienna Standard Mean Ocean Water (V-SMOW).

2.4 Theory and Calculations

2.4.1 Calculations used for the GDGT-based reconstructions

The branched and isoprenoid tetraether (BIT) index is calculated according to Hopmans et al. (2004), for structures see Fig. S5:

$$BIT = \frac{Ia + IIa + IIIa}{Ia + IIa + IIIa + crenarchaeol}. \tag{1}$$

The cyclopentane moiety number of brGDGTs correlates negatively with soil pH (Weijers et al., 2007), which led to the development of the cyclization of branched tetraethers (CBT) ratio. CBT and the CBT based pH (pH$_{CBT}$) were calculated according to Peterse et al. (2012):

$$CBT = -\log \frac{Ib + IIb}{Ia + IIa}, \tag{2}$$

$$pH_{CBT} = 7.9 - 1.97 \times CBT. \tag{3}$$

The number of methyl groups in brGDGTs correlates negatively with T_{MA} and soil pH (Peterse et al., 2012; Weijers et al., 2007). Thus, the ratio of the methylation of branched tetraethers (MBT) ratio and the CBT ratio can be used to reconstruct T_{MA}. We use the equation given by Peterse et al. (2012):

$$MBT' = \frac{Ia + Ib + Ic}{Ia + Ib + Ic + IIa + IIb + IIc + IIIa}, \tag{4}$$

$$T_{MA} = 0.81 - 5.67 \times CBT + 31.0 \times MBT'. \tag{5}$$

2.4.2 Calculations and concepts used for the coupled δ^2H-$\delta^{18}O$ approach

The apparent fractionation is calculated according to Cernusak et al. (2016):

$$\varepsilon_{n\text{-alkane/precipitation}} = \left(\frac{\delta^2H_{n\text{-alkane}} - \delta^2H_{GIPR,OIPC}}{1 + \delta^2H_{GIPR,OIPC}/1000} \right), \tag{6}$$

$$\varepsilon_{sugar/precipitation} = \left(\frac{\delta^{18}O_{sugar} - \delta^{18}O_{GIPR,OIPC}}{1 + \delta^{18}O_{GIPR,OIPC}/1000} \right). \tag{7}$$

The isotopic composition of leaf water ($\delta^2H_{leaf\text{-water}}$ and $\delta^{18}O_{leaf\text{-water}}$) can be calculated using ε_{bio} for $\delta^2H_{n\text{-alkane}}$ (-160‰, Sachse et al., 2012; Sessions et al., 1999) and $\delta^{18}O_{sugar}$ (+27‰, Cernusak et al., 2003; Schmidt et al., 2001):

$$\delta^2H_{leaf\text{-water}} = \left(\frac{1000 + \delta^2H_{n\text{-alkane}}}{1000 + \varepsilon_{bio} (n\text{-alkane})} \right) \times 10^3 - 1000, \tag{8}$$

$$\delta^{18}\text{O}_{\text{leaf-water}}=\left(\frac{1000+\delta^{18}\text{O}_{\text{sugar}}}{1000+\varepsilon_{\text{bio (sugar)}}}\right) \times 10^3\text{-}1000. \tag{9}$$

Zech et al. (2013) introduced the conceptual model for the coupled $\delta^2\text{H}_{n\text{-alkane}}$-$\delta^{18}\text{O}_{\text{sugar}}$ approach in detail. Briefly, the coupled approach is based on the following assumptions (illustrated in Fig. 8): (i) The isotopic composition of precipitation, which is set to be equal to the plant source water, typically plots along the global meteoric water line (GMWL; $\delta^2\text{H} = 8 \times \delta^{18}\text{O} + 10$) in a $\delta^{18}\text{O}$ vs. $\delta^2\text{H}$ space (Craig, 1961); (ii) Source water uptake by plants does not lead to any fractionation (e.g. Dawson et al., 2002), and significant evaporation of soil water can be excluded; (iii) Evapotranspiration leads to enrichment of the remaining leaf water along the local evaporation line (LEL; Allison et al., 1985; Bariac et al., 1994; Walker and Brunel, 1990), compared to the source water taken up by the plant; (iv) The biosynthetic fractionation is assumed to be constant. In addition, isotopic equilibrium between plant source water (~ weighted mean annual precipitation) and the local atmospheric water vapour is assumed. Further assumption concerns the isotope steady-state in the evaporating leaf water reservoir. The coupled approach allows for reconstructing the isotopic composition of plant source water ($\delta^2\text{H}_{\text{source-water}}$ and $\delta^{18}\text{O}_{\text{source-water}}$) from the reconstructed leaf water, by calculating the intercepts of the LELs with the GMWL (Zech et al., 2013). The slope of the LEL (S_{LEL}) can be assessed by the following equation (Gat, 1971):

$$S_{\text{LEL}}= \frac{\varepsilon_2^*+C_k^2}{\varepsilon_{18}^*+ C_k^{18}}, \tag{10}$$

where ε^* are equilibrium isotope fractionation factors and C_k are kinetic fractionation factors. The latter equals to 25.1‰ and 28.5‰, for C_k^2 and C_k^{18}, respectively (Merlivat, 1978). The equilibrium fractionation factors can be derived from empirical equations (Horita and Wesolowski, 1994) by using T_{MDV} values. For two Danish sites T_{MDV} are not available, instead T_{MV} is used here (section 2.2 and Tab. S2).

In a $\delta^{18}\text{O}$-$\delta^2\text{H}$ diagram, the distance of the leaf water from the GMWL define the deuterium-excess of leaf water ($d_{\text{leaf-water}} = \delta^2\text{H}_{\text{leaf-water}} - 8 \times \delta^{18}\text{O}_{\text{leaf-water}}$, according Dansgaard, (1964); Fig. 8). To convert $d_{\text{leaf-water}}$ into mean RH during daytime and vegetation period (RH$_{\text{MDV}}$), a simplified Craig-Gordon model can be applied (Zech et al., 2013):

$$RH=1- \frac{\Delta d}{\varepsilon_2^*-8\times\varepsilon_{18}^*+C_k^2-8\times C_k^{18}}, \tag{11}$$

where Δd is the difference in $d_{\text{leaf-water}}$ and the deuterium-excess of source water ($d_{\text{source-water}}$).

2.5 Statistics

In the statistical analysis we checked sample distributions for normality (Shapiro and Wilk, 1965) and for equal variance (Levene, 1960). If normality and equal variances are given, we perform an Analysis of Variance (ANOVA). If that is not the case, we conduct the non-parametric Kruskal-Wallis Test. ANOVA or Kruskal-Wallis are used to find significant differences (a=0.05) between the vegetation types (deciduous, conifer and grass).

In order to describe the relation along a 1:1 line, the coefficient of correlation (R^2) was calculated as $R^2 = 1 - \sum (\text{modeled - measured})^2 / \sum(\text{measured - measured mean})^2$. The small r^2 is taken as coefficient of correlation of a linear regression between a dependent (y) and

279 explanatory variable(s). The root mean square error (RMSE) of the relationships was calculated

280 as $\text{RMSE} = \sqrt{\left(\frac{1}{n} \cdot \sum(\text{modeled - measured})^2\right)}$. All data plotting and statistical analysis was

281 realized in R (version 3.2.2; R Core Team, 2015).

282

3 Results and Discussion

3.1 GDGT concentrations

285 GDGT Ia has the highest concentration under all vegetation types, followed by GDGT IIa and
286 GDGT IIIa (Fig. 2). GDGT Ib, IIb and Ic occur in minor, GDGT IIc and IIIb only in trace
287 amounts. GDGT IIIc was below the detection limit in most of the samples (Tab. S3). Although
288 other studies document an influence of the vegetation cover on soil temperature and soil water
289 content, which control the microbial community composition in soils (Awe et al., 2015; Liu et
290 al., 2014; Mueller-Niggemann et al., 2016), we find no statistically different pattern of the
291 individual brGDGTs.
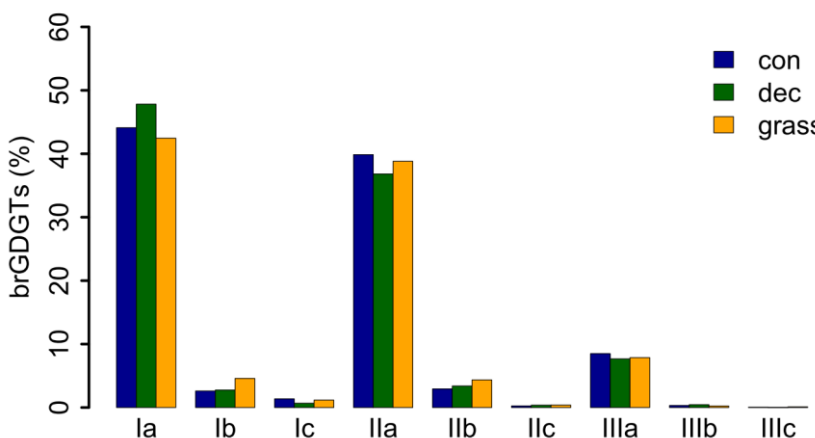
293 **Fig. 2.** Mean concentrations of individual brGDGTs as percentage of all brGDGTs for the three
294 investigated types. Abbreviations: con = coniferous forest sites (n=9); dec = deciduous forest
295 sites (n=14); grass = grassland sites (n=6).

296 Total concentrations of brGDGTs range from 0.32 to 9.17 µg/g dry weight and tend to be
297 highest for the coniferous samples and lowest for the grasses (Fig. 3A, Tab. S3). Bulk brGDGT
298 concentrations lie within the range of other studies examining soils of mid latitude regions
299 (Huguet et al., 2010b, 2010a; Weijers et al., 2011). Similar concentrations in coniferous and
300 deciduous samples imply that brGDGT production does not strongly vary in soils below
301 different forest types. The grass samples show lower brGDGT concentrations compared to the
302 forest samples, but this is probably mainly due to ploughing of the grass sites in former times
303 and hence admixing of mineral subsoil material. The differences in brGDGT concentrations are
304 not significant (p-value = 0.06).

305

3.2 BIT index

307 Most of the samples have a BIT index higher than 0.9 (Fig 3B and Tab. S3). The BIT-values
308 are typical for soils in humid and temperate climate regions (Weijers et al., 2006). However,

309 outliers exist. The most likely source of iGDGTs in soils are Thaumarchaeota, i.e. aerobe
310 ammonia oxidizing archaea producing Crenarchaeol and its regioisomer (Schouten et al., 2013
311 and references therein), when precipitation amount drops below 700-800 mm (Dang et al.,
312 2016; Dirghangi et al., 2013). The P_{MA} data of our sampling sites mostly show precipitation >
313 550 mm (Fig. 1B), but one has to be aware that this data is based on the climate station nearest
314 to the respective sampling locations and microclimate effects, such as sunlight exposure,
315 canopy cover or exposition might have a pronounced influence on the brGDGT vs. iGDGT
316 distribution. Mueller-Niggemann et al. (2016) found higher BIT indices in upland soils
317 compared to paddy soils and stated that the management type also influences BIT values in
318 soils. Along our transect, grass sites tend to have slightly lower BIT-values than forest sites,
319 probably due to the absence of a litter layer and hence, no isolation mechanism preventing
320 evaporation of soil water. Differences between vegetation types are not significant (p-value =
321 0.32).
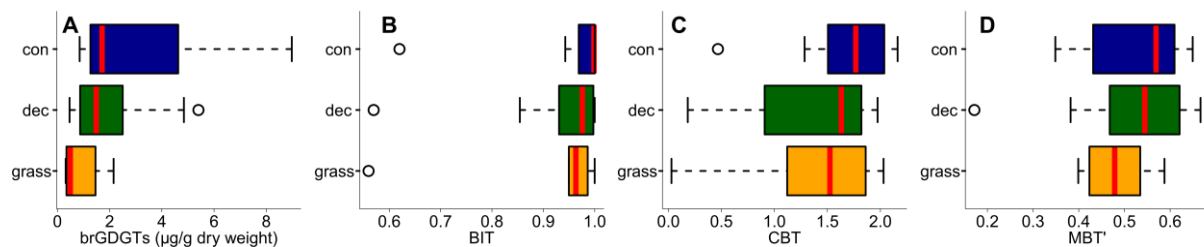
322

Fig. 3. (A) Total concentrations of brGDGTs in µg g^{-1} dry weight, as well as (B) BIT, (C) CBT
and (D) MBT'. Abbreviations: con = coniferous forest sites (n=9); dec = deciduous forest sites
(n=14); grass = grassland sites (n=6). Box plots show median (red line), interquartile range
(IQR) with upper (75%) and lower (25%) quartiles, lowest whisker still within 1.5IQR of lower
quartile, and highest whisker still within 1.5IQR of upper quartile, dots mark outliers.

328

3.3 CBT-derived pH

330 The CBT ratio shows a pronounced variation independent of vegetation type with values
331 between 0.03 and 2.16 (Fig 3C). The coniferous samples tend to be highest, but the differences
332 between vegetation types are not significant (p-value = 0.48). The CBT index can be related to
333 pH in acidic and/or humid soils (e.g. Dirghangi et al., 2013; Mueller-Niggemann et al., 2016;
334 Peterse et al., 2012; Weijers et al., 2007) but might be an indicator of soil water content and
335 hence, precipitation in more arid and alkaline soils (e.g. Dang et al., 2016). There is a
336 pronounced correlation between CBT and soil pH (Fig. 4), which is in good agreement with
337 other studies from mid latitude regions where precipitation is relatively high (Anderson et al.,
338 2014 and references therein). Moreover, the CBT to pH relationship in terms of slope and
339 intersect in our dataset (CBT = -0.47 × pH + 3.5, r^2 = 0.7, p-value < 0.0001, n = 29) is well
340 comparable to the correlation described for the global calibration dataset of Peterse et al. (2012)
341 (CBT = -0.36 × pH + 3.1, r^2 = 0.7, p-value < 0.0001, n = 176).

342 However, there are some outliers in the CBT-pH correlation, which need a further examination
343 (see locations grass L04, dec L10 and dec L12 as marked in Figs. 4 and 5). The outliers show
344 lower BIT indices (< 0.85, Tab. S3). Even though the data from the nearest climate station
345 suggest no abnormal P_{MA}. Local effects such as differences in the amount of sunlight exposure,
346 nutrient availability for brGDGT producing organisms or, most likely soil water content might

influence the brGDGT production at these locations (Anderson et al., 2014; Dang et al., 2016).
A lower BIT index as well as a lower CBT occur when soil water content decreases (Dang et al., 2016; Sun et al., 2016) or when aeration is high and less anoxic microhabitats for GDGT producing microbes exist (e.g. Dirghangi et al., 2013).
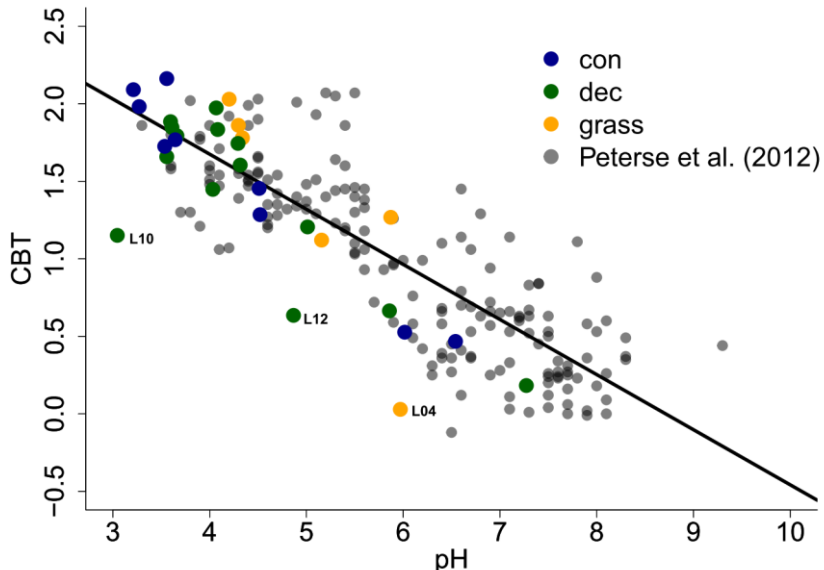
Fig. 4. CBT to pH relationship in our dataset in comparison to the global calibration dataset from Peterse et al. (2012) (CBT = -0.36 × pH + 3.1, r^2 = 0.7, p-value < 0.0001, n = 176, black line). Abbreviations: con = coniferous forest sites (n=9); dec = deciduous forest sites (n=14); grass = grassland sites (n=6).

As the CBT and pH are similarly correlated in our dataset and the global dataset of Peterse et al. (2012), the CBT-derived pH correlated well with the actual pH (Fig. 5A; R^2 = 0.3). Expressed as ΔpH (CBT-derived pH - measured pH), there is a tendency that the GDGTs result in an overestimation of the real pH for the forest sites (Fig. B). Yet a Kruskal-Wallis test shows no statistically significant difference between the vegetation types, with a p-value of 0.13. The overall ΔpH of 0.6 ±0.6 shows that the reconstruction of soil pH using brGDGTs works well along this transect.
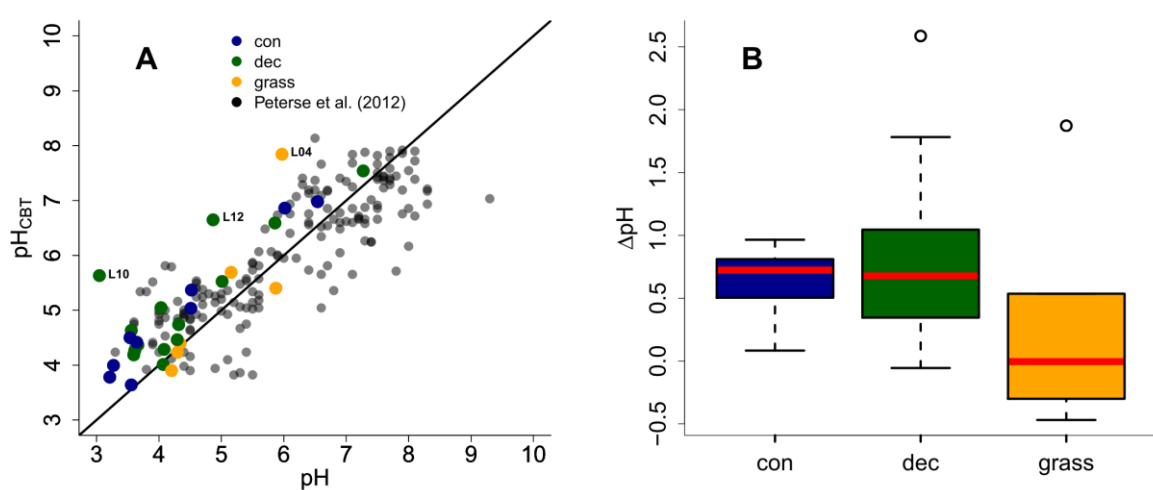
Fig. 5. (A) Correlation between measured pH and reconstructed soil pH (pH$_{CBT}$) from our transect data in comparison to the global calibration dataset from Peterse et al. (2012) ($R^2 = 0.7$, RMSE = 0.75, n = 176). Black line indicates the 1:1 relationship. (B) Boxplots of ΔpH (refers to pH$_{CBT}$-pH). Box plots show median (red line), interquartile range (IQR) with upper (75%) and lower (25%) quartiles, lowest whisker still within 1.5IQR of lower quartile, and highest whisker still within 1.5IQR of upper quartile, dots mark outliers. Abbreviations: con = coniferous forest sites (n=9); dec = deciduous forest sites (n=14); grass = grassland sites (n=6).

3.4 MBT'-CBT-derived T$_{MA}$ reconstructions

The MBT' shows high variability with values ranging from 0.17 to 0.67 no statistical differences between vegetation types (p-value = 0.54; Fig. 3D, Tab. S3). When comparing reconstructed (MBT'-CBT-derived) T$_{MA}$ with climate station T$_{MA}$, the data plot close to the 1:1 line, and fit well into the global dataset of Peterse et al. (2012) (Fig. 6A). The ΔT$_{MA}$ reveal an overall offset of 0.5°C $\pm$2.4 and there is no statistically difference between vegetation types (Fig. 6B). The standard deviation in ΔT$_{MA}$ of $\pm$2.4 is well in line with the RMSE of 5.0 for the global calibration dataset (Peterse et al., 2012).
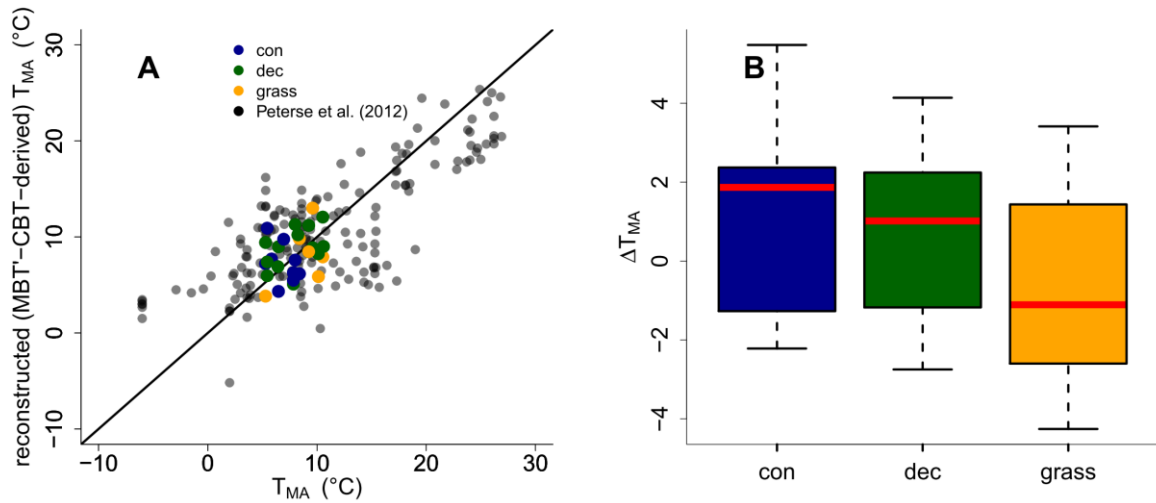
Fig. 6. (A) Correlation between climate station T$_{MA}$ and reconstructed (MBT'-CBT-derived) T$_{MA}$. For comparison, the global calibration dataset from Peterse et al. (2012) is shown. The black line indicates the 1:1 relationship. (B) Boxplots of ΔT$_{MA}$ (refers to reconstructed T$_{MA}$-T$_{MA}$ from climate stations) in the different vegetation types from our transect study. Box plots show median (red line), interquartile range (IQR) with upper (75%) and lower (25%) quartiles, lowest whisker still within 1.5IQR of lower quartile, and highest whisker still within 1.5IQR of upper quartile, dots mark outliers. Abbreviations: con = coniferous forest sites (n=9); dec = deciduous forest sites (n=14); grass = grassland sites (n=6).

3.5 Potential impact of the used liquid chromatography method on pH and T$_{MA}$ reconstructions

The GDGT data presented in this study are not acquired on the up-to-date method (e.g. compare De Jonge et al., 2014 vs. Zech et al., 2012c). De Jonge et al. (2014) presented a new liquid chromatography method which enables the separation for the brGDGTs with m/z 1036, 1034

396 and 1032, 1050, 1048 and 1046 into 6-methyl and 5-methyl stereoisomers. The old method did
397 not allow such a separation (Zech et al., 2012c), thus in the calibration often the sum of 6 and
398 5-methlyted brGDGTs was used (see and compare De Jonge et al., 2014 vs. Peterse et al., 2012).
399 This introduce scatter to the MBT'-CBT-based T_{MA} reconstructions and can cause a correlation
400 between pH and MBT' (for more details see De Jonge et al., 2014). De Jonge et al. (2014)
401 moreover show that the 6-methyl brGDGTs are ubiquitous abundant in soils from all over the
402 world, based on reanalysing the dataset of Peterse et al. (2012). However, they also compare
403 reconstructed T_{MA} values based MBT'-CBT calibration (Peterse et al., 2012) and their new
404 developed T_{MA} calibration and state that they plot around a 1:1 line. They furthermore state,
405 that especially for arid areas larger deviations can be expected. Finally, they conclude that the
406 use of the new developed calibrations will improve the T_{MA} and pH reconstructions for areas
407 with arid climate conditions. Because our study transect spans form southern Germany to
408 southern Sweden, representing temperate and humid climate conditions, we argue that the usage
409 of the older liquid chromatorgraphy method do not introduce a systematic error in our T_{MA} and
410 pH reconstructions. Still, a higher variability/scatter could be associated with the calibration of
411 Peterse et al. (2012) and therefore also present in our T_{MA} and pH reconstructions.

412

413 **3.6 Apparent fractionation of δ^2H and $\delta^{18}O$ in the different vegetation types**
414 δ^2H values could be obtained for the n-alkanes C_{27}, C_{29} and C_{31} in all samples and additionally
415 at two locations for n-C_{25} and n-C_{33} at six other locations. The $\delta^2H_{n\text{-alkane}}$ values, calculated as
416 mean of n-C_{25} to n-C_{31} δ^2H, range from -156 to -216‰. Pooled standard deviations show an
417 overall average of 3.6‰. The $\delta^{18}O_{sugar}$ values, calculated as the area weighted means for
418 arabinose and xylose, range from +27.7 to +39.4‰. The average weighted mean standard
419 deviation is 1.4‰. The compound-specific isotope data are summarized along with the
420 calculations in Tab. S4.

421 Apparent fractionation ($\varepsilon_{n\text{-alkane/precipitation}}$) is on the order of -120 to -150‰, i.e. a bit less than
422 the biosynthetic fraction of -160‰. This implies that evapotranspirative enrichment is ~ 10 to
423 40‰ (Fig. 7A). $\varepsilon_{n\text{-alkane/precipitation}}$ is lower for grass sites compared to the forest sites. Differences
424 are significant between deciduous and grass sites (p-value = 0.005). This finding supports the
425 results of other studies (Kahmen et al., 2013; Liu and Yang, 2008; McInerney et al., 2011), and
426 can be named "signal damping". Grasses do not only incorporate the evaporatively-enriched
427 leaf water but also unenriched xylem water in the growth and differentiation zone of grasses
428 (Gamarra et al., 2016; Liu et al., 2017).

429 The grass-derived hemicellulose sugar biomarkers do not fully record the evapotranspirative
430 enrichment of the leaf water, either, as indicated by lower apparent fractionation ($\varepsilon_{sugar/precipitation}$)
431 in Fig. 7B. The differences are significant between forest and grass sites (p-value < 0.005). This
432 is in agreement with a study on cellulose extracted from grass blades (Helliker and Ehleringer,
433 2002), and again, the "signal damping" can be explained with incorporation of enriched leaf
434 water and non-enriched stem water.

435 Based on the comparison of evapotranspirative enrichment between forest and grass sites, the
436 "signal damping" can be quantified to be ~ 31% for the hemicellulose sugars, and ~ 49% for
437 the n-alkanes. This is in agreement with other studies that reported a loss of 22% of the leaf

438 water enrichment for hemicellulose sugars (Helliker and Ehleringer, 2002) and 39 to 62% loss
439 of the leaf water enrichment for *n*-alkanes (Gamarra et al., 2016).
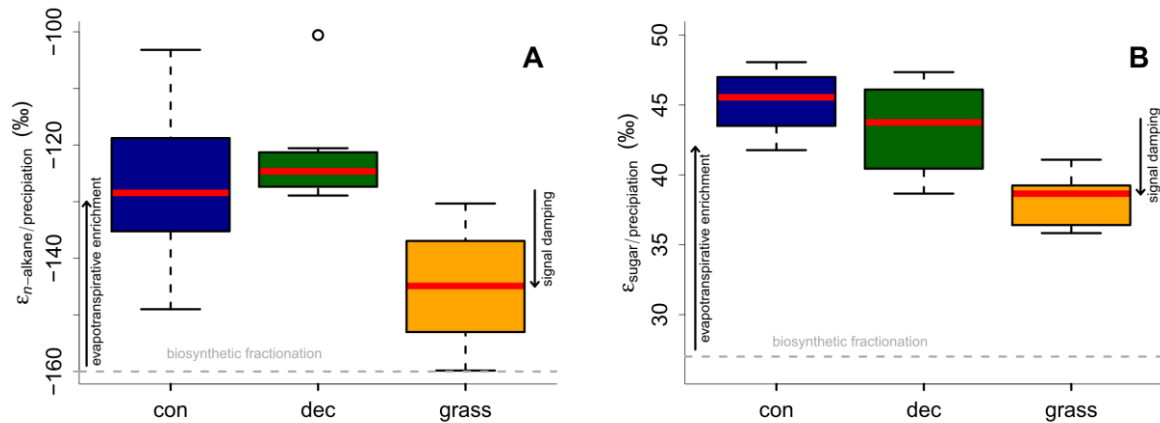
440

441 **Fig. 7.** Apparent fractionation (A) $\varepsilon_{n\text{-alkane/precipitation}}$ and (B) $\varepsilon_{\text{sugar/precipitation}}$. Biosynthetic
442 fractionation factors according to section 2.4.2. Box plots show median (red line), interquartile
443 range (IQR) with upper (75%) and lower (25%) quartiles, lowest whisker still within 1.5IQR
444 of lower quartile, and highest whisker still within 1.5IQR of upper quartile, dots mark outliers.
445 Abbreviations: con = coniferous forest sites (n=9); dec = deciduous forest sites (n=11 and 14
446 for *n*-alkanes and sugars, respectively); grass = grassland sites (n=4 and 6 for *n*-alkanes and
447 sugars, respectively). The figure conceptually illustrates the effect of biosynthetic fractionation
448 and evapotranspirative enrichment as well as "signal damping".

449

450 **3.7 $\delta^2 H_{\text{source-water}}$ and $\delta^{18}O_{\text{source-water}}$ reconstructions**
451 The $\delta^2 H$ versus $\delta^{18}O$ diagram shown in Fig. 8 graphically illustrates the reconstruction of $\delta^2 H_{\text{leaf-water}}$
452 and $\delta^{18}O_{\text{leaf-water}}$ (colored dots) from $\delta^2 H_{n\text{-alkane}}$ and $\delta^{18}O_{\text{sugar}}$ (crosses), as well as the
453 reconstruction of $\delta^2 H_{\text{source-water}}$ and $\delta^{18}O_{\text{source-water}}$ (black dots). For reconstructing $\delta^2 H_{\text{source-water}}$
454 and $\delta^{18}O_{\text{source-water}}$, LELs with an average slope of 2.8 ±0.1 (Eq. 10) can be generated through
455 every leaf water point and the intercepts of these LELs with the GMWL.

456
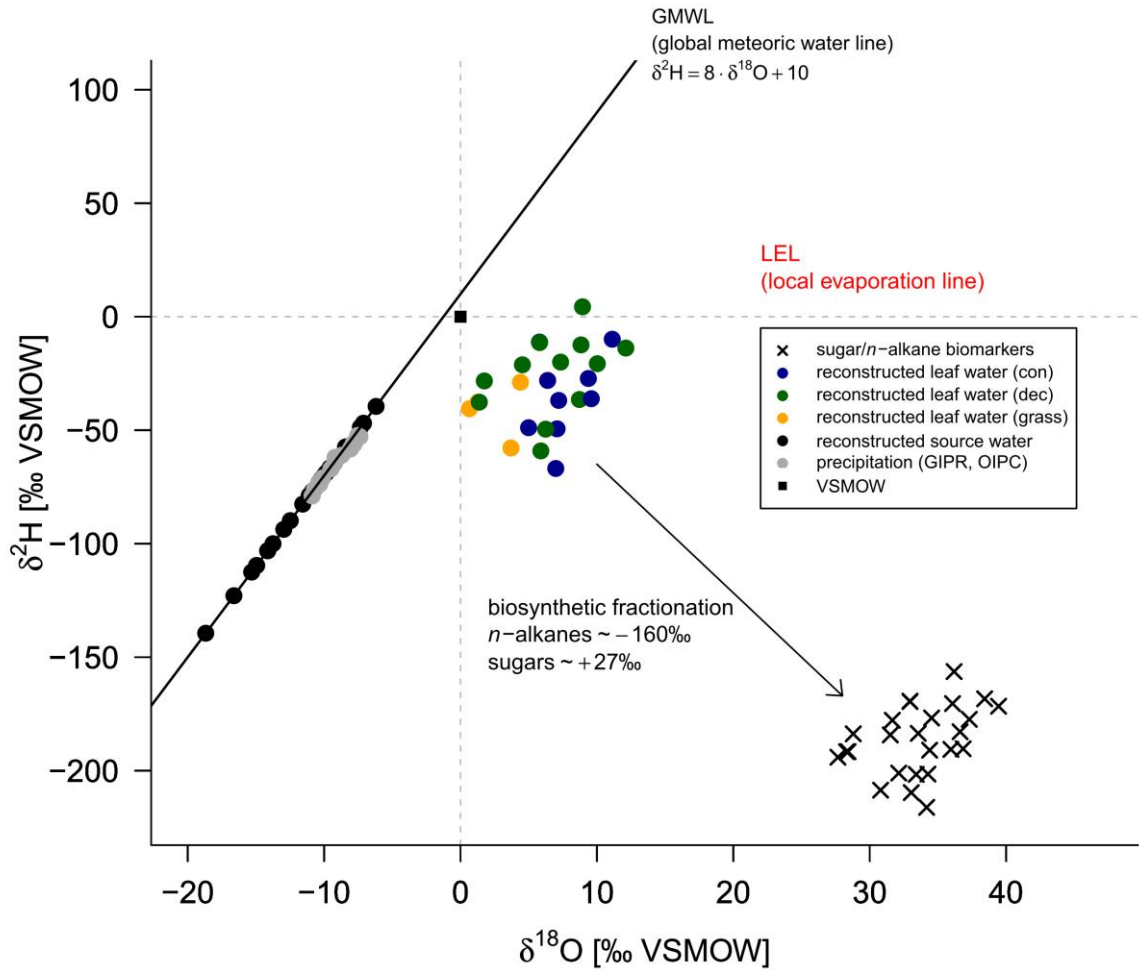
Fig. 8. δ^2H vs. δ^{18}O diagram illustrating the coupled δ^2H$_{n\text{-alkane}}$-δ^{18}O$_{sugar}$ approach: measured
δ^2H$_{n\text{-alkane}}$ and δ^{18}O$_{sugar}$ values, reconstructed δ^2H$_{leaf\text{-water}}$ and δ^{18}O$_{leaf\text{-water}}$ (according Eqs. 8 and
9) and reconstructed δ^2H$_{source\text{-water}}$ and δ^{18}O$_{source\text{-water}}$ in comparison to GIPR and OIPC-based
δ^2H$_{precipitation}$ and δ^{18}O$_{precipitation}$. Abbreviations: con = coniferous forest sites (n=9); dec =
deciduous forest sites (n=11); grass = grassland sites (n=4).

462

The reconstructed δ^2H$_{source\text{-water}}$ and δ^{18}O$_{source\text{-water}}$ results can be compared with the δ^2H$_{GIPR,OIPC}$
and δ^{18}O$_{GIPR,OIPC}$ data (Fig. 9). This comparison reveals that the coupled δ^2H$_{n\text{-alkane}}$-δ^{18}O$_{sugar}$
approach yields more accurate δ^2H$_{source\text{-water}}$ and δ^{18}O$_{source\text{-water}}$ compared to single δ^2H$_{n\text{-alkane}}$
approaches. However, the range of the reconstructed δ^2H$_{source\text{-water}}$ and δ^{18}O$_{source\text{-water}}$ values is
clearly larger than in δ^2H$_{GIPR,OIPC}$ and δ^{18}O$_{GIPR,OIPC}$ values. δ^2H is systematically underestimated
by ~ 21‰ ±22 (Fig. 9B) and δ^{18}O by ~ 2.9‰ ±2.8 (Fig. 9D). The type of vegetation seems to
be not particularly relevant (p-value = 0.18 for $\Delta\delta^2$H and p-value = 0.34 for $\Delta\delta^{18}$O).
Nevertheless, the systematic offsets tend to be lowest for the decidous sites ($\Delta\delta^2$H and $\Delta\delta^{18}$O is
closer to zero with ~-5‰ ±15 and ~-1.1‰ ±2.1), followed by grass sites (~-14‰ ±20 and ~-
2.1‰ ±2.6). In comparison, the coniferous sites show the largest offsets (~-23‰ ±26 for $\Delta\delta^2$H
~-3.0‰ ±3.3 for $\Delta\delta^{18}$O). Differences are, however, not statistically significant. The systematic
offset and the large variability might have more specific reasons, and we suggest that this is
related to the type of vegetation. Deciduous trees produce lots of leaf waxes and sugars (e.g.
Prietzel et al., 2013; Zech et al., 2012a), and all biomarkers reflect and record the

477   evapotranspirative enrichment of the leaf water (e.g. Kahmen et al., 2013; Tuthorn et al., 2014).
478   By contrast, coniferous trees produce quite low amounts of n-alkanes (Diefendorf and Freimuth,
479   2016; Zech et al., 2012a), while sugar concentrations are as high as in other vascular plants (e.g.
480   Hepp et al., 2016; Prietzel et al., 2013). For the coniferous soil samples this means that the n-
481   alkanes stem most likely from the understory whereas the sugars originate from grasses and
482   coniferous needles. When the understory is dominated by grass species then the n-alkane
483   biomarkers do not record the full leaf water enrichment signal, whereas the sugars from the
484   needles do. The reconstructed leaf water for the coniferous sites is therefore too negative
485   concerning δ^2H, and reconstructed $\delta^2H_{source-water}$ and $\delta^{18}O_{source-water}$ values thus also become too
486   negative (Fig. 8). Concerning the grass sites, the following explanation can be found. Correcting
487   for "signal damping" makes the reconstructed leaf water points more positive and shifts them
488   in Fig. 8 up and right. As the "signal damping" is stronger for δ^2H than for $\delta^{18}O$ the corrected
489   leaf water points would now plot above the uncorrected ones. The corrected leaf water points
490   lead to more positive reconstructed $\delta^2H_{source-water}$ and $\delta^{18}O_{source-water}$ values for the grass sites.
491   However, Gao et al. (2014) and Liu et al. (2016) showed that the ε_{bio} (regarding ^2H between n-
492   alkanes and leaf water) of monocotyledon plants could be larger than those of dicotyledonous
493   ones. This would therefore also cause a more negative $\varepsilon_{n\text{-}alkane/precipitation}$ for grasses compared to
494   trees. We observe that the $\varepsilon_{n\text{-}alkane/precipitation}$ is indeed more negative for the grass sites compared
495   to the forest sites (Fig 7 and section 3.6). Therefore, effects of "signal damping" vs. variable
496   ε_{bio} along with vegetation types are indistinguishable here. As an outlook for a future study, we
497   therefore strongly recommend a comparison between the here measured $\delta^2H_{n\text{-}alkane}$ values with
498   modelled ones using e.g. the new available model approach from Konecky et al. (2019), which
499   could provide insights if such vegetation effects on ε_{bio} of ^2H in n-alkanes are describable.

500

501   Vegetation type specific rooting depths could partly cause the overall high variability in
502   reconstructed $\delta^2H_{source-water}$ and $\delta^{18}O_{source-water}$. Deep rooting species most likely use the water
503   from deeper soil horizons and/or shallow ground water, which is equal to the (weighted) mean
504   annual precipitation (e.g. Herrmann et al., 1987). Shallow rooting plants take up water from
505   upper soil horizons, which is influenced by seasonal variations in $\delta^2H_{precipitation}$ and $\delta^{18}O_{precipitation}$
506   and by soil water enrichment (Dubbert et al., 2013). Thus, the overall assumption that the source
507   water of the plants reflects the local (weighted) mean precipitation might be not fully valid for
508   all sites. Moreover, a partly contribution of root-derived rather than leaf-derived sugar
509   biomarkers in our topsoil samples is very likely. This does, by contrast, not apply for n-alkanes,
510   which are hardly produced in roots (Zech et al., 2012b and the discussion therein).
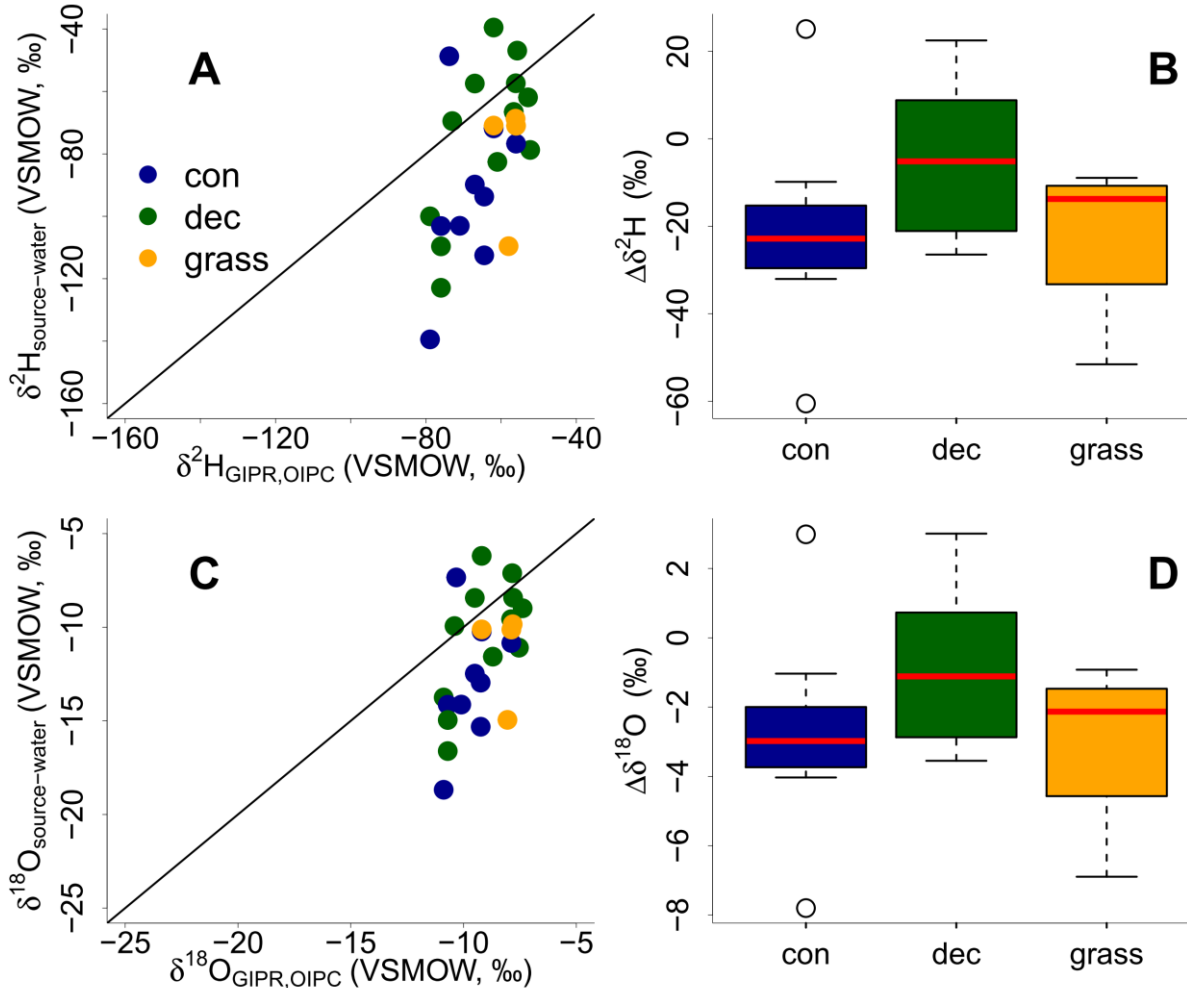
Fig. 9. Correlation of reconstructed $\delta^2H_{source\text{-}water}$ and $\delta^{18}O_{source\text{-}water}$ vs. precipitation $\delta^2H_{GIPR,OIPC}$ and $\delta^{18}O_{GIPR,OIPC}$ (A and C). Black lines indicate 1:1 relationship. Differences between reconstructed source water and precipitation ($\Delta\delta^2H$, $\delta^{18}O = \delta^2H_{source\text{-}water}$, $\delta^{18}O_{source\text{-}water}$ - $\delta^2H_{GIPR,OIPC}$, $\delta^{18}O_{GIPR,OIPC}$) for the three different vegetation types (B and D). Box plots show median (red line), interquartile range (IQR) with upper (75%) and lower (25%) quartiles, lowest whisker still within 1.5IQR of lower quartile, and highest whisker still within 1.5IQR of upper quartile. Abbreviations: con = coniferous forest sites (n=9); dec = deciduous forest sites (n=11); grass = grassland sites (n=4).

Moreover, the high variability within the vegetation types could be caused by variability in ε_{bio} of ^2H in *n*-alkanes, as well as ^{18}O in sugars. There is an ongoing discussion about the correct ε_{bio} for ^{18}O in hemicellulose sugars (Sternberg, 2014 vs. Zech et al., 2014), and ε_{bio} is probably not constant over all vegetation types. This translates into errors concerning leaf water reconstruction and thus for reconstructing $\delta^2H_{source\text{-}water}$ and $\delta^{18}O_{source\text{-}water}$ values (Eq. 9 and Fig. 8). Likewise, the ε_{bio} values reported in the literature for ^2H of *n*-alkanes can be off from -160‰ by tens of permille (Feakins and Sessions, 2010; Tipple et al., 2015; Feakins et al., 2016; Freimuth et al., 2017). The degree to which hydrogen originates from NADPH rather than leaf water is important, because NADPH is more negative (Schmidt et al., 2003). The wide range in biosynthetic ^2H fractionation factors, which can be even larger, is therefore also related to the carbon and energy metabolism state of plants (Cormier et al., 2018).

3.8 RH reconstruction

Reconstructed RH_{MDV} ranges from 34 to 74%, while RH_{MDV} from climate station data range from 61 to 78% (Fig. 10A). Biomarker-based values thus systematically underestimate the station data (ΔRH_{MDV} = -17% ±12). Yet the offsets are much less for deciduous tree and grass sites (ΔRH_{MDV} = -10% ±12 and -7% ±9, respectively; Fig. 10B). The offsets for the coniferous sites are -30% ±11, and significantly larger than for the deciduous and grass sites (p-values < 0.05).

Too low reconstructed RH_{MDV} values for the coniferous sites make sense in view of the previously discussed option that soils contain *n*-alkanes from the understory (which is dominated by grass species), while sugars stem from needles and grasses. As explained earlier already, the "signal damping" leads to too negative reconstructed $\delta^2H_{leaf-water}$ (whereas $\delta^{18}O$ is affected less by the "signal damping"), and too negative $\delta^2H_{leaf-water}$ translates into overestimated d-excess and underestimated RH values. In Fig. 8, a correction for this requires moving the coniferous leaf water data points upwards towards more positive δ^2H values, thus the distance between the leaf water and the source water is reduced. It should be noted that also here variable ε_{bio} (regarding ^2H between *n*-alkanes and leaf water) along with vegetation types could not be distinguished from "signal damping" effects.

The underestimation of RH for the deciduous and grass sites could be partly associated with the use of the GMWL as baseline for the coupled $\delta^2H_{n\text{-alkane}}$-$\delta^{18}O_{sugar}$ approach. The deuterium-excess of the LMWLs is generally lower than the +10‰ of the GMWL, while the slopes of the LMWLs are well comparable to the GMWL (Stumpp et al., 2014). In addition, if soil water evaporation occurred before water uptake by the plants, this would lead to an underestimation of biomarker-based RH_{MDV} values, too. It can be furthermore assumed that plant metabolism is highest during times with direct sunshine and high irradiation, i.e. during noon at sunny days. The relevant RH could therefore be lower than the climate station-derived RH_{MDV}. Indeed, already climate station RH_{MDV} is considerably lower than RH_{MA} and RH_{MV} (Tab. S1).
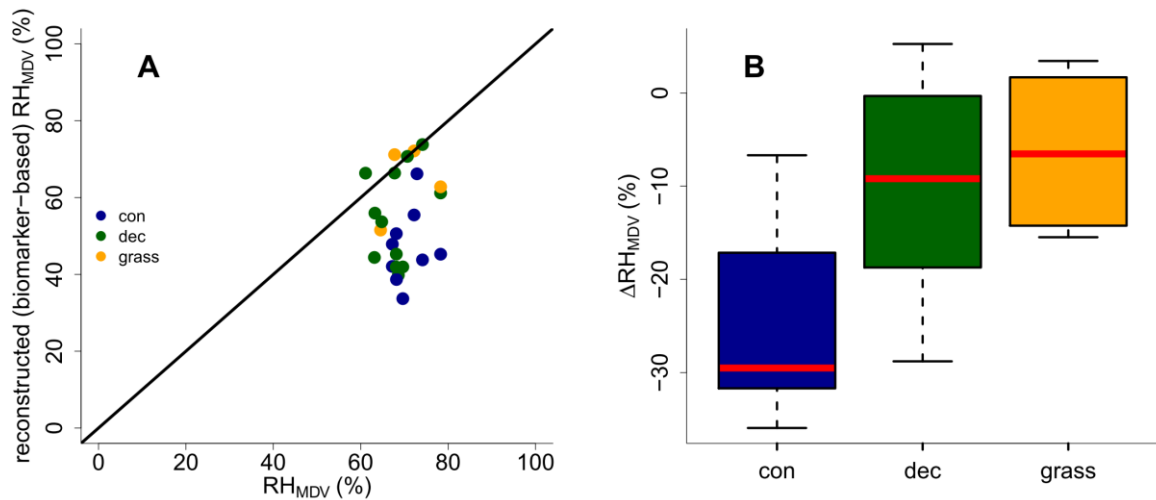
Fig. 10. (A) Comparison of reconstructed (biomarker-based) RH_{MDV} values and climate station RH_{MDV} data. The black line indicates the 1:1 relationship. (B) Differences between reconstructed and climate station RH_{MDV} values (ΔRH_{MDV} = reconstructed − climate station RH_{MDV}) for the three different vegetation types along the transect. Abbreviations: con = coniferous forest sites (n=9); dec = deciduous forest sites (n=11); grass = grassland sites (n=4).

563   The uncertainty of reconstructed RH_{MDV} values are large for all three investigated vegetation
564   types, and again these uncertainties are probably also related to ε_{bio}, which is most likely not
565   constant as assumed for our calculations. Moreover, microclimate variability is underestimated
566   in our approach. As mentioned in the sections 2.4.2 and 3.7, in the coupled approach not only
567   the source water of the plants is equated with (weighted) mean annual precipitation, but also an
568   isotopic equilibrium between the source water and the (local) atmospheric water vapour is
569   assumed. However, in areas with distinct seasonality this might be not fully valid. To account
570   for this lack of equilibrium between precipitation and local atmospheric water vapour, apparent
571   ε values can be calculated with data from Jacob and Sonntag (1991). As shown by Hepp et al.
572   (2018) those values can be used to achieve alternative RH reconstructions based on the coupled
573    $\delta^2H_{n\text{-alkane}}$-$\delta^{18}O_{sugar}$ approach. Such calculated RH_{MDV} values are on average 1.5% more
574   negative than the original values. However, this difference in RH is far below the analytical
575   uncertainties of the compound-specific biomarker isotope analysis.

576   Finally, the integration time of the investigated topsoils has to be discussed. Unfortunately, no
577   ^{14}C dates are available for the soil samples. However, most likely the organic matter has been
578   built up over a longer timescale than the available climate data, which is used for comparison.
579   In combination with vegetation changes/management changes throughout that period, this
580   could surely lead to a less tight relationship of the reconstructions compared to the climate
581   station data. Root input of arabinose and xylose seems to be of minor relevance in our topsoil
582   samples. Otherwise, the reconstructed $\delta^{18}O_{sugar}$ values would be too negative resulting in
583   RH_{MDV} overestimations, which is not observed.

584

4 Conclusions

586   We were able to show that

587   (i)   the vegetation type does not significantly influence the brGDGT concentrations and
588   proxies, yet the coniferous sites tend to have higher brGDGT concentrations, BIT
589   indices and CBT-MBT' ratios, while grass sites tend to be lowest.
590   (ii)   CBT faithfully records soil pH with a median ΔpH of 0.6 ± 0.6, The CBT
591   overestimates the real pH particularly at the forest sites.
592   (iii)   CBT-MBT'-derived T_{MA} reflect the climate station-derived T_{MA} values with a
593   median ΔT_{MA} of 0.5°C ± 2.4, but again slightly too high reconstructions for the forest
594   sites were observed.
595   (iv)   differences in the apparent fractionation between the investigated vegetation types
596   can be explained with "signal damping".
597   (v)   the reconstructed $\delta^2H_{source\text{-}water}$ and $\delta^{18}O_{source\text{-}water}$ reflect the $\delta^2H_{GIPR,OIPC}$ and
598               $\delta^{18}O_{GIPR,OIPC}$ with a systematic offset for δ^2H of ~-21‰ ± 22 and for $\delta^{18}O$ of ~-2.9‰
599   ± 2.8 (based on overall medians of $\Delta\delta^2H$, $\Delta\delta^{18}O$). This is caused by too negative
600   reconstructions for coniferous and grass sites. For coniferous sites, this can be
601   explained with n-alkanes originating from understory grasses. As for the grass sites,
602   the "signal damping" or variable ε_{bio} along with vegetation types effect δ^2H more
603   than $\delta^{18}O$. This leads to too negative reconstructed $\delta^2H_{leaf\text{-}water}$ values and thus to too
604   negative $\delta^2H_{source\text{-}water}$ and $\delta^{18}O_{source\text{-}water}$ reconstructions.

(vi) reconstructed (biomarker-based) RH_{MDV} values tend to underestimate climate station-derived RH_{MDV} values (ΔRH_{MDV} = ~ -17% ±12). For coniferous sites the underestimations are strongest, which can be explained with understory grasses being the main source of *n*-alkanes for the investigated soils under coniferous forests.

Overall, our study highlights the great potential of brGDGTs and the coupled $\delta^2H_{n\text{-alkane}}$-$\delta^{18}O_{sugar}$ approach for more quantitative paleoclimate reconstructions. Taking into account effects of different vegetation types improves correlations and reconstructions. This holds particularly true for the coupled $\delta^2H_{n\text{-alkane}}$-$\delta^{18}O_{sugar}$ approach, which is affected by "signal damping" of the grass vegetation or variable ε_{bio} (regarding ^2H between *n*-alkanes and leaf water) along with vegetation types. By contrast, vegetation-related effects do not strongly influence the brGDGT-derived reconstructions. Assuming constant ε_{bio} is likely a considerable source of uncertainty and should be further addressed in future field and/or modelling studies. Climate chamber experiments are most promising to further evaluate and refine the coupled $\delta^2H_{n\text{-alkane}}$-$\delta^{18}O_{sugar}$ approach, because uncertainties related to microclimate variability can be reduced. Field experiments like ours suffer from the fact that biomarker pools in the sampled topsoils may have been affected by past vegetation and climate changes and by the rather small range covered by the sampled transect. Both makes the comparison between reconstructions and observations more difficult compared to large datasets und well defined conditions.

Acknowledgements

We thank L. Wüthrich, H. Veit, T. Sprafke, A. Groos (all University of Bern), A. Kühnel (Technical University of Munich) for constructive discussions and statistical advices, and M. Schaarschmidt (University of Bayreuth), C. Heinrich and M. Benesch (Martin-Luther-University Halle-Wittenberg) for laboratory assistance during $\delta^{18}O_{sugar}$ analysis and pH measurements, respectively. The Swiss National Science Foundation (PP00P2 150590) funded this research. J. Hepp greatly acknowledges the support by the German Federal Environmental Foundation (DBU) in form of his PhD-fellowship. This publication was funded by the German Research Foundation (DFG) and the University of Bayreuth in the funding programme Open Access Publishing.

References

Allison, G. B., Gat, J. R. and Leaney, F. W. J.: The relationship between deuterium and oxygen-18 delta values in leaf water, Chemical Geology, 58, 145–156, 1985.

Amelung, W., Cheshire, M. V. and Guggenberger, G.: Determination of neutral and acidic sugars in soil by capillary gas-liquid chromatography after trifluoroacetic acid hydrolysis, Soil Biology and Biochemistry, 28(12), 1631–1639, 1996.

Anderson, V. J., Shanahan, T. M., Saylor, J. E., Horton, B. K. and Mora, A. R.: Sources of local and regional variability in the MBT'/CBT paleotemperature proxy: Insights from a modern elevation transect across the Eastern Cordillera of Colombia, Organic Geochemistry, 69, 42–51, doi:10.1016/j.orggeochem.2014.01.022, 2014.

Awe, G. O., Reichert, J. M. and Wendroth, O. O.: Temporal variability and covariance structures of soil temperature in a sugarcane field under different management practices in southern Brazil, Soil and Tillage Research, 150, 93–106, doi:10.1016/j.still.2015.01.013, 2015.

Bariac, T., Gonzalez-Dunia, J., Katerji, N., Béthenod, O., Bertolini, J. M. and Mariotti, A.: Spatial variation of the isotopic composition of water (^{18}O, ^{2}H) in the soil-plant-atmosphere system, 2. Assessment under field conditions, Chemical Geology, 115, 317–333, 1994.

Bowen, G. J.: The Online Isotopes in Precipitation Calculator, version 3.1., 2018.

Bowen, G. J. and Revenaugh, J.: Interpolating the isotopic composition of modern meteoric precipitation, Water Resources Research, 39(10), 1–13, doi:10.1029/2003WR002086, 2003.

Brincat, D., Yamada, K., Ishiwatari, R., Uemura, H. and Naraoka, H.: Molecular-isotopic stratigraphy of long-chain *n*-alkanes in Lake Baikal Holocene and glacial age sediments, Organic Geochemistry, 31(4), 287–294, doi:10.1016/S0146-6380(99)00164-3, 2000.

Cappelen, J.: Danish Climatological Normals 1971-2000 - for selected stations., 2002.

Cernusak, L. A., Wong, S. C. and Farquhar, G. D.: Oxygen isotope composition of phloem sap in relation to leaf water in Ricinus communis, Functional Plant Biology, 30(10), 1059–1070, 2003.

Cernusak, L. A., Barbour, M. M., Arndt, S. K., Cheesman, A. W., English, N. B., Feild, T. S., Helliker, B. R., Holloway-Phillips, M. M., Holtum, J. A. M., Kahmen, A., Mcinerney, F. A., Munksgaard, N. C., Simonin, K. A., Song, X., Stuart-Williams, H., West, J. B. and Farquhar, G. D.: Stable isotopes in leaf water of terrestrial plants, Plant Cell and Environment, 39(5), 1087–1102, doi:10.1111/pce.12703, 2016.

Christoph, H., Eglinton, T. I., Zech, W., Sosin, P. and Zech, R.: A 250 ka leaf-wax δD record from a loess section in Darai Kalon , Southern Tajikistan, Quaternary Science Reviews, 208, 118–128, doi:10.1016/j.quascirev.2019.01.019, 2019.

Coffinet, S., Huguet, A., Anquetil, C., Derenne, S., Pedentchouk, N., Bergonzini, L., Omuombo, C., Williamson, D., Jones, M., Majule, A. and Wagner, T.: Evaluation of branched GDGTs and leaf wax n-alkane δ^{2}H as (paleo) environmental proxies in East Africa, Geochimica et Cosmochimica Acta, 198, 182–193, doi:10.1016/j.gca.2016.11.020, 2017.

Cormier, M.-A., Werner, R. A., Sauer, P. E., Gröcke, D. R., M.C., L., Wieloch, T., Schleucher, J. and Kahmen, A.: ^{2}H fractiontions during the biosynthesis of carbohydrates and lipids imprint a metabolic signal on the δ^{2}H values of plant organic compounds, New Phytologist, 218(2), 479–491, doi:10.1111/nph.15016, 2018.

Craig, H.: Isotopic Variations in Meteoric Waters, Science, 133, 1702–1703, 1961.

Dang, X., Yang, H., Naafs, B. D. A., Pancost, R. D. and Xie, S.: Evidence of moisture control on the methylation of branched glycerol dialkyl glycerol tetraethers in semi-arid and arid soils, Geochimica et Cosmochimica Acta, 189, 24–36, doi:10.1016/j.gca.2016.06.004, 2016.

Dansgaard, W.: Stable isotopes in precipitation, Tellus, 16(4), 436–468, doi:10.1111/j.2153-3490.1964.tb00181.x, 1964.

689   Dawson, T. E., Mambelli, S., Plamboeck, A. H., Templer, P. H. and Tu, K. P.: Stable Isotopes
690   in Plant Ecology, Annual Review of Ecology and Systematics, 33(1), 507–559,
691   doi:10.1146/annurev.ecolsys.33.020602.095451, 2002.

692   Diefendorf, A. F. and Freimuth, E. J.: Extracting the most from terrestrial plant-derived *n*-alkyl
693   lipids and their carbon isotopes from the sedimentary record: A review, Organic
694   Geochemistry, 103(January), 1–21, doi:10.1016/j.orggeochem.2016.10.016, 2016.

695   Dirghangi, S. S., Pagani, M., Hren, M. T. and Tipple, B. J.: Distribution of glycerol dialkyl
696   glycerol tetraethers in soils from two environmental transects in the USA, Organic
697   Geochemistry, 59, 49–60, doi:10.1016/j.orggeochem.2013.03.009, 2013.

698   Dubbert, M., Cuntz, M., Piayda, A., Maguás, C. and Werner, C.: Partitioning evapotranspiration
699   - Testing the Craig and Gordon model with field measurements of oxygen isotope ratios
700   of   evaporative   fluxes,   Journal   of   Hydrology,   496,   142–153,
701   doi:10.1016/j.jhydrol.2013.05.033, 2013.

702   DWD Climate Data Center: Historical annual precipitation observations for Germany. [online]
703   Available   from: ftp://ftp-
704   cdc.dwd.de/pub/CDC/observations_germany/climate/hourly/precipitation/historical/
705   (Accessed 20 September 2018a), 2018.

706   DWD Climate Data Center: Historical hourly station observations of 2m air temperature and
707   humidity   for   Germany.   [online]   Available   from: ftp://ftp-
708   cdc.dwd.de/pub/CDC/observations_germany/climate/hourly/air_temperature/historical/
709   (Accessed 19 September 2018b), 2018.

710   Eglinton, T. I. and Eglinton, G.: Molecular proxies for paleoclimatology, Earth and Planetary
711   Science Letters, 275(1), 1–16, 2008.

712   Feakins, S. J. and Sessions, A. L.: Controls on the D/H ratios of plant leaf waxes in an arid
713   ecosystem,   Geochimica   et   Cosmochimica   Acta,   74(7),   2128–2141,
714   doi:http://dx.doi.org/10.1016/j.gca.2010.01.016, 2010.

715   Feakins, S. J., Bentley, L. P., Salinas, N., Shenkin, A., Blonder, B., Goldsmith, G. R., Ponton,
716   C., Arvin, L. J., Wu, M. S., Peters, T., West, A. J., Martin, R. E., Enquist, B. J., Asner, G.
717   P. and Malhi, Y.: Plant leaf wax biomarkers capture gradients in hydrogen isotopes of
718   precipitation from the Andes and Amazon, Geochimica et Cosmochimica Acta, 182, 155–
719   172, doi:10.1016/j.gca.2016.03.018, 2016.

720   Freimuth, E. J., Diefendorf, A. F. and Lowell, T. V.: Hydrogen isotopes of *n*-alkanes and *n*-
721   alkanoic acids as tracers of precipitation in a temperate forest and implications for
722   paleorecords,   Geochimica   et   Cosmochimica   Acta,   206,   166–183,
723   doi:10.1016/j.gca.2017.02.027, 2017.

724   Frich, P., Rosenørn, S., Madsen, H. and Jensen, J. J.: Observed Precipitation in Denmark, 1961-
725   90., 1997.

726   Gamarra, B., Sachse, D. and Kahmen, A.: Effects of leaf water evaporative ^{2}H-enrichment and
727   biosynthetic fractionation on leaf wax *n*-alkane δ^2H values in C3 and C4 grasses, Plant,
728   Cell and Environment Environment, 39, 2390–2403, doi:10.1111/pce.12789, 2016.

729   Gao, L., Edwards, E. J., Zeng, Y. and Huang, Y.: Major evolutionary trends in hydrogen isotope
730   fractionation   of   vascular   plant   leaf   waxes,   PLoS   ONE,   9(11),
731   doi:10.1371/journal.pone.0112610, 2014.

Gat, J. R.: Comments on the Stable Isotope Method in Regional Groundwater Investigations, Water Resources Research, 7(4), 980–993, doi:10.1029/WR007i004p00980, 1971.

van Geldern, R., Baier, A., Subert, H. L., Kowol, S., Balk, L. and Barth, J. A. C.: (Table S1) Stable isotope composition of precipitation sampled at Erlangen, Germany between 2010 and 2013 for station GeoZentrum located at Erlangen city center, in In supplement to: van Geldern, R et al. (2014): Pleistocene paleo-groundwater as a pristine fresh water resource in southern Germany – evidence from stable and radiogenic isotopes. Science of the Total Environment, 496, 107-115, https://doi.org/10.1016/j., PANGAEA., 2014.

Guggenberger, G., Christensen, B. T. and Zech, W.: Land-use effects on the composition of organic matter in particle-size separates of soil: I. Lignin and carbohydrate signature, European Journal of Soil Science, 45(December), 449–458, 1994.

Helliker, B. R. and Ehleringer, J. R.: Grass blades as tree rings: environmentally induced changes in the oxygen isotope ratio of cellulose along the length of grass blades, New Phytologist, 155, 417–424, 2002.

Hepp, J., Rabus, M., Anhäuser, T., Bromm, T., Laforsch, C., Sirocko, F., Glaser, B. and Zech, M.: A sugar biomarker proxy for assessing terrestrial versus aquatic sedimentary input, Organic Geochemistry, 98, 98–104, doi:10.1016/j.orggeochem.2016.05.012, 2016.

Hepp, J., Wüthrich, L., Bromm, T., Bliedtner, M., Schäfer, I. K., Glaser, B., Rozanski, K., Sirocko, F., Zech, R. and Zech, M.: How dry was the Younger Dryas? Evidence from a coupled δ^2H-δ^{18}O biomarker paleohygrometer, applied to the Lake Gemündener Maar sediments, Western Eifel, Germany, Climate of the Past Discussions, (September), 1–44, doi:10.5194/cp-2018-114, 2018.

Herrmann, A., Maloszewski, P. and Stichler, W.: Changes of ^{18}O contents of precipitation water during seepage in the unsaturated zone, in Proceedings of International Symposium on Groundwater Monitoring and Management, 23 - 28 March, p. 22, Institut of Water Management Berlin (GDR) with support of UNESCO, Dresden., 1987.

Hopmans, E. C., Weijers, J. W. H., Schefuß, E., Herfort, L., Sinninghe Damsté, J. S. and Schouten, S.: A novel proxy for terrestrial organic matter in sediments based on branched and isoprenoid tetraether lipids, Earth and Planetary Science Letters, 224(1–2), 107–116, doi:10.1016/j.epsl.2004.05.012, 2004.

Horita, J. and Wesolowski, D. J.: Liquid-vapor fractionation of oxygen and hydrogen isotopes of water from the freezing to the critical temperature, Geochimica et Cosmochimica Acta, 58(16), 3425–3437, doi:http://dx.doi.org/10.1016/0016-7037(94)90096-5, 1994.

Hothorn, T., Bühlmann, P., Dudoit, S., Molinaro, A. and Van Der Laan, M. J.: Survival ensembles, Biostatistics, 7(3), 355–373, doi:10.1093/biostatistics/kxj011, 2006.

Hou, J., D'Andrea, W. J. and Huang, Y.: Can sedimentary leaf waxes record D/H ratios of continental precipitation? Field, model, and experimental assessments, Geochimica et Cosmochimica Acta, 72, 3503–3517, doi:10.1016/j.gca.2008.04.030, 2008.

Huguet, A., Fosse, C., Metzger, P., Fritsch, E. and Derenne, S.: Occurrence and distribution of extractable glycerol dialkyl glycerol tetraethers in podzols, Organic Geochemistry, 41(3), 291–301, doi:10.1016/j.orggeochem.2009.10.007, 2010a.

Huguet, A., Fosse, C., Laggoun-Défarge, F., Toussaint, M. L. and Derenne, S.: Occurrence and distribution of glycerol dialkyl glycerol tetraethers in a French peat bog, Organic Geochemistry, 41(6), 559–572, doi:10.1016/j.orggeochem.2010.02.015, 2010b.

776   IAEA/WMO: Global Network of Isotopes in Precipitation. The GNIP Database., 2015.

777   IAEA/WMO: Global Network of Isotopes in Precipitation. The GNIP Database., 2018.

778   Jacob, H. and Sonntag, C.: An 8-year record of the seasonal- variation of ^{2}H and ^{18}O in
779   atmospheric water vapor and precipitation at Heidelberg, Tellus, 43B(3), 291–300, 1991.

780   De Jonge, C., Hopmans, E. C., Zell, C. I., Kim, J. H., Schouten, S. and Sinninghe Damsté, J.
781   S.: Occurrence and abundance of 6-methyl branched glycerol dialkyl glycerol tetraethers
782   in soils: Implications for palaeoclimate reconstruction, Geochimica et Cosmochimica
783   Acta, 141, 97–112, doi:10.1016/j.gca.2016.03.038, 2014.

784   Kahmen, A., Schefuß, E. and Sachse, D.: Leaf water deuterium enrichment shapes leaf wax n-
785   alkane δD values of angiosperm plants I: Experimental evidence and mechanistic
786   insights, Geochimica et Cosmochimica Acta, 111, 39–49, doi:10.1016/j.gca.2012.09.004,
787   2013.

788   Knapp, D. R.: Handbook of Analytical Derivatization Reactions, John Wiley & Sons, New
789   York, Chichester, Brisbane, Toronto, Singapore., 1979.

790   Konecky, B., Dee, S. G. and Noone, D. C.: WaxPSM: A Forward Model of Leaf Wax Hydrogen
791   Isotope Ratios to Bridge Proxy and Model Estimates of Past Climate, Journal of
792   Geophysical Research: Biogeosciences, 124, 2107–2125, doi:10.1029/2018JG004708,
793   2019.

794   Laursen, E. V., Thomsen, R. S. and Cappelen, J.: Observed Air Temperature, Humidity,
795   Pressure, Cloud Cover and Weather in Denmark - with Climatological Standard Normals,
796   1961-90., 1999.

797   Levene, H.: Robust Tests for Equality of Variances, in Contributions to Probability and
798   Statistics: Essays in Honor of Harold Hotelling, vol. 69, edited by I. Olkin, pp. 78–92,
799   Standford University Press, Palo Alto, California., 1960.

800   Liu, J., Liu, W., An, Z. and Yang, H.: Different hydrogen isotope fractionations during lipid
801   formation in higher plants: Implications for paleohydrology reconstruction at a global
802   scale, Scientific Reports, 6, 19711, doi:10.1038/srep19711, 2016.

803   Liu, W. and Yang, H.: Multiple controls for the variability of hydrogen isotopic compositions
804   in higher plant n-alkanes from modern ecosystems, Global Change Biology, 14(9), 2166–
805   2177, doi:10.1111/j.1365-2486.2008.01608.x, 2008.

806   Liu, Y., Wang, J., Liu, D., Li, Z., Zhang, G., Tao, Y., Xie, J., Pan, J. and Chen, F.: Straw
807   mulching reduces the harmful effects of extreme hydrological and temperature conditions
808   in citrus orchards, PLoS ONE, 9(1), 1–9, doi:10.1371/journal.pone.0087094, 2014.

809   McInerney, F. A., Helliker, B. R. and Freeman, K. H.: Hydrogen isotope ratios of leaf wax n-
810   alkanes in grasses are insensitive to transpiration, Geochimica et Cosmochimica Acta,
811   75(2), 541–554, doi:10.1016/j.gca.2010.10.022, 2011.

812   Merlivat, L.: Molecular diffusivities of $H_2^{16}O$, $HD^{16}O$, and $H_2^{18}O$ in gases, The Journal of
813   Chemical Physics, 69(6), 2864–2871, doi:http://dx.doi.org/10.1063/1.436884, 1978.

814   Mueller-Niggemann, C., Utami, S. R., Marxen, A., Mangelsdorf, K., Bauersachs, T. and
815   Schwark, L.: Distribution of tetraether lipids in agricultural soils - Differentiation
816   between paddy and upland management, Biogeosciences, 13(5), 1647–1666,
817   doi:10.5194/bg-13-1647-2016, 2016.

818 Oppermann, B. I., Michaelis, W., Blumenberg, M., Frerichs, J., Schulz, H. M., Schippers, A.,
819   Beaubien, S. E. and Krüger, M.: Soil microbial community changes as a result of long-
820   term exposure to a natural CO_2 vent, Geochimica et Cosmochimica Acta, 74(9), 2697–
821   2716, doi:10.1016/j.gca.2010.02.006, 2010.

822 Pedentchouk, N. and Zhou, Y.: Factors Controlling Carbon and Hydrogen Isotope Fractionation
823   During Biosynthesis of Lipids by Phototrophic Organisms, in Hydrocarbons, Oils and
824   Lipids: Diversity, Origin, Chemistry and Fate. Handbook of Hydrocarbon and Lipid
825   Microbiology, edited by H. Wilkes, pp. 1–24, Springer, Cham., 2018.

826 Peterse, F., van der Meer, J., Schouten, S., Weijers, J. W. H., Fierer, N., Jackson, R. B., Kim,
827   J. H. and Sinninghe Damsté, J. S.: Revised calibration of the MBT-CBT paleotemperature
828   proxy based on branched tetraether membrane lipids in surface soils, Geochimica et
829   Cosmochimica Acta, 96, 215–229, doi:10.1016/j.gca.2012.08.011, 2012.

830 Prietzel, J., Dechamps, N. and Spielvogel, S.: Analysis of non-cellulosic polysaccharides helps
831   to reveal the history of thick organic surface layers on calcareous Alpine soils, Plant and
832   Soil, 365(1–2), 93–114, doi:10.1007/s11104-012-1340-2, 2013.

833 R Core Team: R: A Language and Environment for Statistical Computing, [online] Available
834   from: https://www.r-project.org/, 2015.

835 Rach, O., Brauer, A., Wilkes, H. and Sachse, D.: Delayed hydrological response to Greenland
836   cooling at the onset of the Younger Dryas in western Europe, Nature Geoscience, 7(1),
837   109–112, doi:10.1038/ngeo2053, 2014.

838 Rao, Z., Zhu, Z., Jia, G., Henderson, A. C. G., Xue, Q. and Wang, S.: Compound specific δD
839   values of long chain *n*-alkanes derived from terrestrial higher plants are indicative of the
840   δD of meteoric waters: Evidence from surface soils in eastern China, Organic
841   Geochemistry, 40(8), 922–930, doi:http://dx.doi.org/10.1016/j.orggeochem.2009.04.011,
842   2009.

843 Romero-Viana, L., Kienel, U. and Sachse, D.: Lipid biomarker signatures in a hypersaline lake
844   on Isabel Island (Eastern Pacific) as a proxy for past rainfall anomaly (1942-2006AD),
845   Palaeogeography, Palaeoclimatology, Palaeoecology, 350–352, 49–61,
846   doi:10.1016/j.palaeo.2012.06.011, 2012.

847 Sachse, D., Radke, J. and Gleixner, G.: Hydrogen isotope ratios of recent lacustrine sedimentary
848   *n*-alkanes record modern climate variability, Geochimica et Cosmochimica Acta, 68(23),
849   4877–4889, doi:http://dx.doi.org/10.1016/j.gca.2004.06.004, 2004.

850 Sachse, D., Radke, J. and Gleixner, G.: δD values of individual *n*-alkanes from terrestrial plants
851   along a climatic gradient – Implications for the sedimentary biomarker record, Organic
852   Geochemistry, 37, 469–483, doi:10.1016/j.orggeochem.2005.12.003, 2006.

853 Sachse, D., Billault, I., Bowen, G. J., Chikaraishi, Y., Dawson, T. E., Feakins, S. J., Freeman,
854   K. H., Magill, C. R., McInerney, F. A., van der Meer, M. T. J., Polissar, P., Robins, R. J.,
855   Sachs, J. P., Schmidt, H.-L., Sessions, A. L., White, J. W. C. and West, J. B.: Molecular
856   Paleohydrology: Interpreting the Hydrogen-Isotopic Composition of Lipid Biomarkers
857   from Photosynthesizing Organisms, Annual Reviews, 40, 221–249,
858   doi:10.1146/annurev-earth-042711-105535, 2012.

859 Schäfer, I. K., Lanny, V., Franke, J., Eglinton, T. I., Zech, M., Vysloužilová, B. and Zech, R.:
860   Leaf waxes in litter and topsoils along a European transect, SOIL, 2, 551–564,
861   doi:10.5194/soil-2-551-2016, 2016.

862 Schlotter, D.: The spatio-temporal distribution of $\delta^{18}O$ and δ^2H of precipitation in Germany -
863   an evaluation of regionalization methods, Albert-Ludwigs-Universität Freiburg im
864   Breisgau.   [online]   Available   from: http://www.hydrology.uni-
865   freiburg.de/abschluss/Schlotter_D_2007_DA.pdf, 2007.

866 Schmidt, H.-L., Werner, R. A. and Roßmann, A.: ^{18}O Pattern and biosynthesis of natural plant
867   products,   Phytochemistry,   58(1),   9–32,   doi:http://dx.doi.org/10.1016/S0031-
868   9422(01)00017-6, 2001.

869 Schmidt, H.-L., Werner, R. A. and Eisenreich, W.: Systematics of ^2H patterns in natural
870   compounds   and   its   importance   for   the   elucidation   of   biosynthetic   pathways,
871   Phytochemistry Reviews, 2(1–2), 61–85, doi:10.1023/B:PHYT.0000004185.92648.ae,
872   2003.

873 Schouten, S., Hopmans, E. C. and Sinninghe Damsté, J. S.: The organic geochemistry of
874   glycerol dialkyl glycerol tetraether lipids: A review, Organic Geochemistry, 54, 19–61,
875   doi:10.1016/j.orggeochem.2012.09.006, 2013.

876 Schreuder, L. T., Beets, C. J., Prins, M. A., Hatté, C. and Peterse, F.: Late Pleistocene climate
877   evolution in Southeastern Europe recorded by soil bacterial membrane lipids in Serbian
878   loess,   Palaeogeography,   Palaeoclimatology,   Palaeoecology,   449,   141–148,
879   doi:10.1016/j.palaeo.2016.02.013, 2016.

880 Sessions, A. L., Burgoyne, T. W., Schimmelmann, A. and Hayes, J. M.: Fractionation of
881   hydrogen isotopes in lipid biosynthesis, Organic Geochemistry, 30, 1193–1200, 1999.

882 Shapiro, S. S. and Wilk, M. B.: An Analysis of Variance Test for Normality, Biometrika,
883   52(3/4), 591–611, doi:/biomet/52.3-4.591, 1965.

884 Sternberg, L. S. L.: Comment on "Oxygen isotope ratios ($^{18}O/^{16}O$) of hemicellulose-derived
885   sugar biomarkers in plants, soils and sediments as paleoclimate proxy I: Insight from a
886   climate chamber experiment" by Zech et al. (2014), Geochimica et Cosmochimica Acta,
887   141, 677–679, doi:10.1016/j.gca.2014.04.051, 2014.

888 Strobl, C., Boulesteix, A. L., Zeileis, A. and Hothorn, T.: Bias in random forest variable
889   importance measures: Illustrations, sources and a solution, BMC Bioinformatics, 8,
890   doi:10.1186/1471-2105-8-25, 2007.

891 Strobl, C., Boulesteix, A. L., Kneib, T., Augustin, T. and Zeileis, A.: Conditional variable
892   importance for random forests, BMC Bioinformatics, 9, 1–11, doi:10.1186/1471-2105-9-
893   307, 2008.

894 Stumpp, C., Klaus, J. and Stichler, W.: Analysis of long-term stable isotopic composition in
895   German   precipitation,   Journal   of   Hydrology,   517,   351–361,
896   doi:10.1016/j.jhydrol.2014.05.034, 2014.

897 Sun, C. J., Zhang, C. L., Li, F. Y., Wang, H. Y. and Liu, W. G.: Distribution of branched
898   glycerol dialkyl glycerol tetraethers in soils on the Northeastern Qinghai-Tibetan Plateau
899   and possible production by nitrite-reducing bacteria, Science China Earth Sciences, 59(9),
900   1834–1846, doi:10.1007/s11430-015-0230-2, 2016.

901 Swedish Meteorological and Hydrological Institute: SMHI Open Data Meteorological
902   Observations., 2018.

903 Tipple, B. J., Berke, M. A., Hambach, B., Roden, J. S. and Ehleringer, J. R.: Predicting leaf
904   wax n-alkane $^2H/^1H$ ratios: Controlled water source and humidity experiments with

hydroponically grown trees confirm predictions of Craig-Gordon model, Plant, Cell and Environment, 38(6), 1035–1047, doi:10.1111/pce.12457, 2015.

Tuthorn, M., Zech, M., Ruppenthal, M., Oelmann, Y., Kahmen, A., del Valle, H. F., Wilcke, W. and Glaser, B.: Oxygen isotope ratios (^{18}O/^{16}O) of hemicellulose-derived sugar biomarkers in plants, soils and sediments as paleoclimate proxy II: Insight from a climate transect study, Geochimica et Cosmochimica Acta, 126, 624–634, doi:http://dx.doi.org/10.1016/j.gca.2013.11.002, 2014.

Tuthorn, M., Zech, R., Ruppenthal, M., Oelmann, Y., Kahmen, A., del Valle, H. F., Eglinton, T., Rozanski, K. and Zech, M.: Coupling δ^2H and δ^{18}O biomarker results yields information on relative humidity and isotopic composition of precipitation - a climate transect validation study, Biogeosciences, 12, 3913–3924, doi:10.5194/bg-12-3913-2015, 2015.

Umweltbundesamt GmbH: Erhebung der Wassergüte in Österreich gemäß Hydrographiegesetz i.d.F. des BGBl. Nr. 252/90 (gültig bis Dezember 2006) bzw. Gewässerzustandsüberwachung in Österreich gemäß Wasserrechtsgesetz, BGBl. I Nr. 123/06, i.d.g.F.; BMLFUW, Sektion IV / Abteilung 3 N. [online] Available from: https://wasser.umweltbundesamt.at/h2odb/fivestep/abfrageQdPublic.xhtml (Accessed 20 September 2018), 2018.

Walker, C. D. and Brunel, J.-P.: Examining Evapotranspiration in a Semi-Arid Region using Stable Isotopes of Hydrogen and Oxygen, Journal of Hydrology, 118, 55–75, 1990.

Wang, C., Hren, M. T., Hoke, G. D., Liu-Zeng, J. and Garzione, C. N.: Soil n-alkane δD and glycerol dialkyl glycerol tetraether (GDGT) distributions along an altitudinal transect from southwest China: Evaluating organic molecular proxies for paleoclimate and paleoelevation, Organic Geochemistry, 107, 21–32, doi:10.1016/j.orggeochem.2017.01.006, 2017.

Wang, H., Liu, W., Zhang, C. L., Liu, Z. and He, Y.: Branched and isoprenoid tetraether (BIT) index traces water content along two marsh-soil transects surrounding Lake Qinghai: Implications for paleo-humidity variation, Organic Geochemistry, 59, 75–81, doi:10.1016/j.orggeochem.2013.03.011, 2013.

Weijers, J. W. H., Schouten, S., Spaargaren, O. C. and Sinninghe Damsté, J. S.: Occurrence and distribution of tetraether membrane lipids in soils: Implications for the use of the TEX$_{86}$ proxy and the BIT index, Organic Geochemistry, 37(12), 1680–1693, doi:10.1016/j.orggeochem.2006.07.018, 2006.

Weijers, J. W. H., Schouten, S., van den Donker, J. C., Hopmans, E. C. and Sinninghe Damsté, J. S.: Environmental controls on bacterial tetraether membrane lipid distribution in soils, Geochimica et Cosmochimica Acta, 71(3), 703–713, doi:10.1016/j.gca.2006.10.003, 2007.

Weijers, J. W. H., Wiesenberg, G. L. B., Bol, R., Hopmans, E. C. and Pancost, R. D.: Carbon isotopic composition of branched tetraether membrane lipids in soils suggest a rapid turnover and a heterotrophic life style of their source organism(s), Biogeosciences, 7(9), 2959–2973, doi:10.5194/bg-7-2959-2010, 2010.

Weijers, J. W. H., Steinmann, P., Hopmans, E. C., Schouten, S. and Sinninghe Damsté, J. S.: Bacterial tetraether membrane lipids in peat and coal: Testing the MBT-CBT temperature proxy for climate reconstruction, Organic Geochemistry, 42(5), 477–486, doi:10.1016/j.orggeochem.2011.03.013, 2011.

950 Xie, S., Pancost, R. D., Chen, L., Evershed, R. P., Yang, H., Zhang, K., Huang, J. and Xu, Y.:
951   Microbial lipid records of highly alkaline deposits and enhanced aridity associated with
952   significant uplift of the Tibetan Plateau in the Late Miocene, Geology, 40(4), 291–294,
953   doi:10.1130/G32570.1, 2012.

954 Zech, M. and Glaser, B.: Compound-specific $\delta^{18}O$ analyses of neutral sugars in soils using gas
955   chromatography-pyrolysis-isotope ratio mass spectrometry: problems, possible solutions
956   and a first application, Rapid Communications in Mass Spectrometry, 23, 3522–3532,
957   doi:10.1002/rcm, 2009.

958 Zech, M., Rass, S., Buggle, B., Löscher, M. and Zöller, L.: Reconstruction of the late
959   Quaternary paleoenvironments of the Nussloch loess paleosol sequence, Germany, using
960   n-alkane   biomarkers,   Quaternary   Research,   78(2),   226–235,
961   doi:10.1016/j.yqres.2012.05.006, 2012a.

962 Zech, M., Kreutzer, S., Goslar, T., Meszner, S., Krause, T., Faust, D. and Fuchs, M.: Technical
963   Note: *n*-Alkane lipid biomarkers in loess: post-sedimentary or syn-sedimentary?,
964   Discussions, Biogeosciences, 9, 9875–9896, doi:10.5194/bgd-9-9875-2012, 2012b.

965 Zech, M., Tuthorn, M., Detsch, F., Rozanski, K., Zech, R., Zöller, L., Zech, W. and Glaser, B.:
966   A 220 ka terrestrial $\delta^{18}O$ and deuterium excess biomarker record from an eolian
967   permafrost   paleosol   sequence,   NE-Siberia,   Chemical   Geology,
968   doi:10.1016/j.chemgeo.2013.10.023, 2013.

969 Zech, M., Mayr, C., Tuthorn, M., Leiber-Sauheitl, K. and Glaser, B.: Reply to the comment of
970   Sternberg on "Zech et al. (2014) Oxygen isotope ratios ($^{18}O/^{16}O$) of hemicellulose-
971   derived sugar biomarkers in plants, soils and sediments as paleoclimate proxy I: Insight
972   from a climate chamber experiment. GCA, Geochimica et Cosmochimica Acta, 141(0),
973   680–682, doi:10.1016/j.gca.2014.04.051, 2014.

974 Zech, M., Zech, R., Rozanski, K., Gleixner, G. and Zech, W.: Do *n*-alkane biomarkers in
975   soils/sediments reflect the $\delta^{2}H$ isotopic composition of precipitation? A case study from
976   Mt . Kilimanjaro and implications for paleoaltimetry and paleoclimate research, Isotopes
977   in   Environmental   and   Health   Studies,   51(4),   508–524,
978   doi:10.1080/10256016.2015.1058790, 2015.

979 Zech, R., Gao, L., Tarozo, R. and Huang, Y.: Branched glycerol dialkyl glycerol tetraethers in
980   Pleistocene loess-paleosol sequences: Three case studies, Organic Geochemistry, 53, 38–
981   44, doi:10.1016/j.orggeochem.2012.09.005, 2012c.